https://doi.org/10.5194/egusphere-2026-4466
Preprint. Discussion started: 27 August 2026

Glacial controls on iron and manganese concentration and lability in an Arctic fjord

Łukasz Stachnik[1,2], Meri Korhonen[3], Jonathan R. Hawkings[4,5], Marlena Szeligowska[6], Katarzyna Koziorowska[6], Emilia Trudnowska[6], Karol Kuliński[6], Beata Szymczycha[6], Oskar Głowacki[3], Małgorzata Kitowska[6], Katarzyna Dragańska-Deja[6], Marcin Syczewski[2,7], Liane G. Benning[2,8], Pablo Forjanes[2], Mateusz Moskalik[3]

[1]Alfred Jahn Cold Regions Research Centre, University of Wrocław, 50-383, Wrocław, Poland
[2] GFZ, Helmholtz Centre for Geosciences, 14473, Potsdam, Germany
[3]Institute of Geophysics, Polish Academy of Sciences, Warszawa, Poland
[4]University of Pennsylvania, 19104-6316, Philadelphia, USA
[5]iC3, The Arctic University of Norway, Tromsø, Norway
[6]Institute of Oceanology Polish, Academy of Sciences, 81-712, Sopot, Poland
[7] Faculty of Biology, University of Warsaw, 02-096, Warszawa, Poland
[8] Department of Earth Sciences, Freie Universität Berlin, 12249, Berlin, Germany

Correspondence to: Lukasz Stachnik (lukasz.stachnik@uwr.edu.pl)

Abstract. Retreating glaciers are altering sediment and micronutrient fluxes to coastal waters, yet the magnitude and environmental impacts of change remain unclear. Here we examine how contrasting glacier systems in an Arctic fjord control the export and speciation of dissolved and particulate iron (Fe) and manganese (Mn) by comparing locations influenced by marine-terminating and land-terminating glaciers. Data was collected from two glacierized bays in Hornsund, a southern Svalbard fjord, during research cruises conducted in 2022 and 2023. Highly reactive ascorbate-extractable particulate Fe was a major component of the Fe pool in both systems, exceeding dissolved Fe even beyond the inner coastal zone, indicating that reactive particulate Fe is transported farther offshore than previously assumed. The marine-terminating glacier influenced bay exhibited substantially higher concentrations of reactive particulate Fe and Mn, elevated dissolved Mn, and sedimentation rates one to two orders of magnitude greater than in the bay with a land-terminating glacier. These differences might be a result of higher subglacial discharge, a larger glacier cover with enhanced chemical weathering, and a higher abundance of freshly weathered mineral surfaces in the marine-terminating glacier influenced bay. In contrast, the input of suspended particulate matter and reactive micronutrient phases from the land-terminating system was lower, as advanced glacial retreat has led to stabilisation of proglacial sediments and the glacier is smaller. Based on this dataset, coastal micronutrient inputs are likely to decline as glaciers continue to retreat, due to falling glacier discharge and supply of reactive sediment enriched in reactive micronutrients.

1 Introduction

Arctic warming is accelerating glacier mass loss, enhancing meltwater discharge, and increasing the delivery of sediments and solutes to fjords and coastal seas (Hugonnet et al., 2021). These changes alter physical, chemical and biological gradients from land to ocean (Hawkings et al., 2026; Hopwood et al., 2020). Glacierised Arctic fjords, shaped by strong salinity and turbidity gradients, are environments where glacial inputs undergo biogeochemical transformation before reaching the coastal ocean. As glaciers retreat and hydrological systems change, the magnitude and form of sediment and nutrient transfer are expected to shift, yet the implications for Arctic coastal biogeochemistry remain insufficiently understood (Kavan et al., 2025; Kochtitzky et al., 2022).

https://doi.org/10.5194/egusphere-2026-4466
Preprint. Discussion started: 27 August 2026

Although many studies have examined macronutrient (N, P, Si) dynamics in glacier-influenced waters, far fewer have addressed the transport and fate of micronutrients such as iron (Fe) and manganese (Mn), despite their central role in regulating marine primary production and carbon cycling in polar regions (Browning and Moore, 2023; Browning et al., 2021). Fe and Mn limitation is widespread in the Southern Ocean (Browning et al., 2021; Tagliabue et al., 2017) and occurs seasonally in the North Atlantic (Krisch et al., 2020; Ryan-Keogh et al., 2013; Hawley et al., 2026; Achterberg et al., 2018). In fjord environments, research has traditionally focused on the dissolved Fe and Mn pools comprising both truly dissolved and/or colloidal/nanoparticulate phases. These fractions are strongly modified by estuarine removal through particle scavenging (Statham et al., 2008; Kanna et al., 2020). However, recent work indicates that chemically reactive particulate Fe and Mn, typically dominated by Fe and Mn oxyhydroxides, nanoparticulate Fe(II)-rich phases, and surface-bound phases, constitute a major export pathway from glacierised catchments (Hawkings et al., 2018; Forsch et al., 2021; Jones et al., 2025). Measurements of reactive particulate Fe and Mn rely on operationally defined extraction procedures, each with inherent uncertainties related to mineralogical heterogeneity, nanoparticle aggregation, and dissolution of refractory phases. Riverine studies show that reactive particulate Fe can exceed dissolved concentrations by orders of magnitude (Hawkings et al., 2018; Pryer et al., 2020; Stachnik et al., 2025), and Fe(II)-rich glacial supended particulate matter (SPM) can stimulate marine phytoplankton production (Shoenfelt et al., 2017; Wyatt et al., 2023). Despite growing evidence of the importance of reactive particulate Fe and Mn, the mechanisms controlling their production, transformation, and fate along the land–ocean continuum remain poorly constrained, especially seasonality in these dynamic environments, for which observational datasets remain limited.

In the Arctic, ongoing recession of marine-terminating glaciers toward land-terminating states is reshaping the pathways through which sediments and solute enter fjords. Deep Greenlandic fjords with marine-terminating glaciers promote strong entrainment of nutrient-rich subsurface waters into buoyant plumes, supplying macronutrients to the upper water layers (Meire et al., 2016; Meire et al., 2017; Cape et al., 2019). In contrast, land-terminating glaciers deliver meltwater and sediments primarily at the surface layer, intensifying stratification and turbidity while weakening vertical nutrient replenishment (Halbach et al., 2019; Hopwood et al., 2018). There is also a strong body of evidence showing that early diagenesis in glacially derived fjord benthic sediments results in the release of iron and manganese to the water column (Herbert et al., 2020; Laufer-Meiser et al., 2020; Ng et al., 2022; Wehrmann et al., 2014; Piret et al., 2026). Biogeochemical variability across glacier types and sizes is likely to modify the reactivity and flux of particulates (Forsch et al., 2025; Van Genuchten et al., 2021), but the extent of this modification and its seasonal control on Fe/Mn cycling in Arctic fjords remain largely unquantified.

Here, we use observations collected in 2022 and 2023 in two bays in Hornsund (a fjord in Svalbard, European Arctic) to determine how contrasting glacial-bay settings within an Arctic fjord – with the main difference being marine-terminating and land-terminating glaciers - shape the export, phase, and seasonal dynamics of dissolved and reactive particulate Fe and Mn. We hypothesise that the larger, more hydrologically active, marine-terminating glacier exports freshly produced, more chemically reactive Fe and Mn material whereas the smaller land-terminating system exports more weathered, less reactive material associated with proglacial storage and a small subglacial catchment area.

https://doi.org/10.5194/egusphere-2026-4466
Preprint. Discussion started: 27 August 2026

2 Study area

Hornsund is a heavily glacierized fjord in southwestern Svalbard (Fig. 1). The study areas, Hansbukta and Gåshamna, lie ~15 km apart in the outer part of Hornsund but differ in glaciology, hydrography and geomorphology. Hansbukta, on the northern coast of Hornsund, receives substantial meltwater and suspended sediment from the marine-terminating Hansbreen (Korhonen et al., 2024). The bay reaches ~90 m depth and is partly isolated from the main fjord by a shallow 15–20 m deep sill located ~3 km from the glacier front (Ćwiąkała et al., 2018). The sill restricts water exchange between Hansbukta and the main fjord and enhances the retention of glacially derived freshwater and particles close to the glacier terminus (Moskalik et al., 2018; Pajda et al., 2026). In contrast, Gåshamna is a shallow (~30 m), open embayment on the southern coast of Hornsund with no sill, supplied primarily by meltwater streams from the land-terminating Gåsbreen.

Hansbreen (77°05′N, 15°37′E) covers 51.3 km^2 (Błaszczyk et al., 2019), and has lost ~40 % of its area since 1936 (Nuth et al., 2015). Increasing atmospheric and seawater temperatures contributed to the retreat of the glacier front by 917 m from 1992-2015 (Błaszczyk et al., 2021). The glacier has a mean elevation of 291 m a.s.l. (Błaszczyk et al., 2013). Gåsbreen (76°54′N, 16°02′E) covered approximately 10.9 km^2 in 2020 (Dudek et al., 2023) with a total catchment area of 38.3 km^2 (Schmidt et al., 2023). Gåsbreen has decreased in area by 26 % between 1938 and2020 (Dudek and Pętlicki, 2023; Dudek et al., 2023), but an increasing surface debris cover is now lowering melt rates (Patel et al., 2026). Gåsbreen has a higher mean elevation than Hansbreen (407 m a.s.l.) (Błaszczyk et al., 2013). Glacier ablation for Hansbreen is ~106 10^6 m^3, which is ~5 times higher than Gåsbreen (Błaszczyk et al., 2013). In 1991-2024, runoff from the Hansbreen catchment was on average 91 10^6 m^3 (45-175 10^6 m3), which was ~2 times higher than the Gåsbreen catchment, with snowmelt from the proglacial area of Gåsbreen contributing a substantial part of the runoff, rather than glacial melt alone (Schmidt and Schuler, 2024; Schmidt et al., 2023).

Both glacier catchments are underlain by Neoproterozoic basement rocks, dominated by foliated schists, phyllites, quartzites and marbles of the Sofiebogen and related groups. In both basins, these metamorphic units are overlain in the eastern sectors by Cambrian carbonate successions of the Sørkapp Land Group, forming a sharp lithostratigraphic boundary between deformed basement and younger sedimentary cover. While this relationship is broadly similar, the Gåsbreen catchment displays a more explicit stratigraphic succession, with Carboniferous sandstones unconformably overlying the older metamorphic series in its western part (Birkenmajer, 1990; Czerny et al., 1992; Dallmann and Elvevold, 2015).

https://doi.org/10.5194/egusphere-2026-4466
Preprint. Discussion started: 27 August 2026

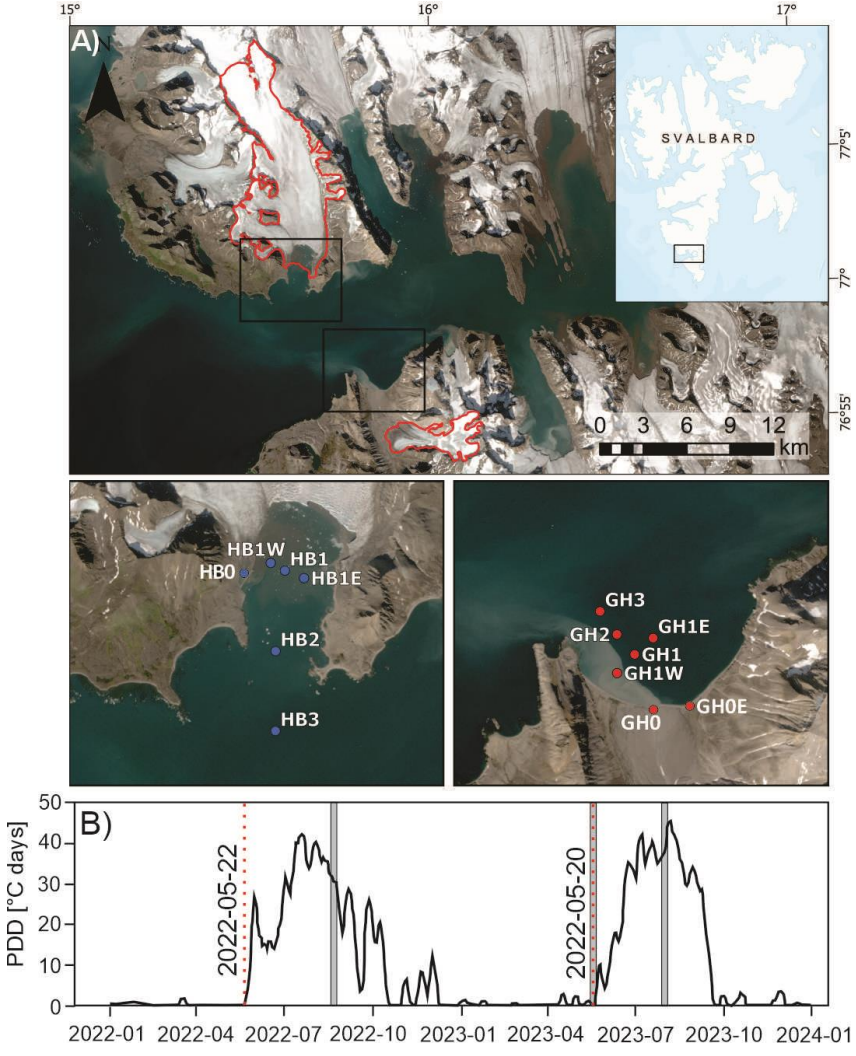

Fig. 1. A) Location of the study area in the Hornsund fjord, Svalbard. Blue and red points mark the location of sampling in 2022 and 2023. B) Seasonal sum of Positive Degree Days (PDD) for June-August, calculated at 6-day intervals for Hornsund. Vertical grey lines indicate sampling days during the summer of 2022 and spring and summer of 2023, and the dashed red lines indicate the start of the summer melt season, which began on 22 May in 2022 and 20 May in 2023. Source: TopoSvalbard, Nowergian Polar Institute.

3 Methods

3.1 Fieldwork and sample preparation

3.1.2 Water sampling and supplementary measurements

The data used in this study were collected during three separate cruises on board the sailing yacht Azimuth. The cruises took place in August 2022, May 2023, and July-August 2023. The locations and number of stations sampled varied slightly between the cruises (Fig. 1). In August 2022, two stations were investigated in Hansbukta (HB1, HB2, Fig. 1): one in Hansbukta and one over the bathymetric sill. In Gåshamna, observations were made at two

https://doi.org/10.5194/egusphere-2026-4466
Preprint. Discussion started: 27 August 2026

locations with varying distance from the coast. In May and July-August 2023, the observations in Hansbukta consisted of five stations: three in Hansbukta, parallel to the glacier terminus, one over the sill and one just outside of Hansbukta, close to the sill. The shallow bathymetric sill likely restricts the water exchange (Moskalik et al., 2018; Pajda et al., 2026) and hence the station furthest from the terminus of Hansbreen may rather represent the properties of the main Hornsund fjord and not those of inner Hansbukta. In Gåshamna, the measurement locations in 2023 were similar to those in Hansbukta, with three stations parallel to the coastline and two further out. However, in May 2023, only one station close to the coastline was visited (GH1, Fig. 1). Additionally, river water samples were collected at the mouths of rivers discharging into Gåshamna (Gåsbreen river, GH0, GHE0) and Hansbukta (Hansbreen river, HB0).

To complement the dataset, suspended particulate matter (SPM) samples and sediment traps from the long-term oceanographic monitoring programme in the Hornsund fjord from 2022-2025 were also included (Korhonen et al., 2024). These supplementary data provide additional context for temporal variability in particulate loads within the fjord system. SPM data from monitoring programme were collected at stations located close to HB1 and GH1 (Fig. 1).

At each station, depending on the depth of the station, water samples were collected at depths of 1, 5, 15, 25, 35, 50 and 5 m over the bottom using a bathymetric rosette equipped with 3.5 L Niskin bottles (Hydrobios, Germany). The rosette consisted of a stainless-steel frame and was deployed using a polypropylene wire. CTD (conductivity-temperature-depth) casts used an RBRconcerto (RBR Ltd), deployed on a polypropylene wire before water sampling with the Niskin rosette. The CTD operated with a sampling rate of 2 Hz and a descent velocity of 0.3-0.5 m/s. Both down- and up-cast were used for averaging the data to 1-dbar vertical bins.

3.1.2 Filtration and sample treatment

For selected sites and depths, suspended particulate matter samples (SPM) for sequential extraction were taken from ~1 L of water filtered through 25 mm pre-weighted Whatman™ polyethersulfone (PES) membrane filters (0.45 µm pore size). PES filters were air-dried and placed in a clean plastic polystyrene Petri dish. For SEM analyses, separate water samples were filtered through track-etched polycarbonate filters (Sartorius™; 0.2 µm pore size).

During the three cruises and the long-term oceanographic monitoring programme in Hornsund fjord, data on SPM concentration as well as sediment flux from 2022-2025, were obtained. As the observations in the monitoring programme span the whole melt season, which typically lasts from May to October, the data provides a more robust picture of seasonality than the yacht cruises alone. Sediment flux measurements were obtained from sediment traps deployed sequentially for 1 to 10 days. SPM samples were collected when sediment traps were deployed and/or recovered. The water samples for both SPM and sedimentation rate were filtered through glass fibre membrane filters (GF/F 25 mm, 0.7 µm pore size). After filtration, GF/F filters were rinsed with ultrapure water (Milli-Q UPW; 18.2 MΩ cm^{-1}) to avoid sea salt recrystallisation. After filtration the exact volume of filtered water, excluding filtration with UPW, was noted. Detailed description of the water sampling associated with the oceanographic monitoring in Hornsund fjord can be found in supplementary materials (Text S1.1) and in Korhonen et al. (2024). During yacht cruises, water samples (~1 L) for SPM concentration were filtered in a similar manner as during monitoring. The GF/F filters were placed in the freezer immediately after filtration.

https://doi.org/10.5194/egusphere-2026-4466
Preprint. Discussion started: 27 August 2026

For analyses of operationally defined dissolved trace elements (d[element]), water was transferred directly from the Niskin bottle via acid-washed silicone tubing using a peristaltic pump to acid-washed Whatman GD/XP syringe filters (pore size 0.45 µm) into acid-washed 125 ml Low Density Polyethylene bottles (LDPE). Before filtration, the hose and syringe filter were flushed with sample water (~200 ml). After filtration, water samples were acidified to 0.2 % v/v with ultrapure hydrochloric acid (Fisher Chemicals™, Optima™). Filtration and acidification of water samples were performed in a field HEPA-filtered laminar flow hood to limit airborne contamination. In addition, unfiltered water was collected in 125 ml LDPE bottles for selected samples and acidified immediately in the field for determination of total dissolvable elements (Td[element]). The samples were re-filtered using Whatman GD/XP syringe filters (0.45 µm pore size) into 125 mL LDPE bottles approximately one month after sample collection. All sampling equipment were cleaned before use. LDPE bottles and silicone tubing were cleaned as follows: 24 h in 1% DECON™ solution, 5 times UPW, 48 h in 10% v/v analytical grade HCl ROMIL™, with a final 5 time rinse in UPW. Bottles were dried in a laminar flow hood. Syringe filters were rinsed with 10% v/v ultrapure hydrochloric acid (Fisher Chemicals™, Optima™) with acid left in the syringe filter for 2 h, and afterwards washed with MQ water.

3.2 Analysis of dissolved and sediment-bound trace elements

3.2.1 Iron and manganese extraction from SPM

Highly reactive iron (assumed to be freshly precipitated poorly ordered ferrihydrite nanoparticles and surface bound Fe^{2+}) was extracted by a buffered ascorbic acid solution, and more crystalline iron (oxy)hydroxides (predominantly aged ferrihydrite, lepidocrocite, hematite and goethite) were extracted using a buffered dithionite solution, as detailed by (Raiswell et al., 2018; Raiswell et al., 2010). These methods are also selective for Mn minerals and have been used for marine sediments and suspended particulate matter (Lenstra et al., 2021; Lenstra et al., 2020; Lenstra et al., 2022).

Ascorbic acid, to a final concentration of 0.057 M, was added to a deoxygenated solution of 0.17 M sodium citrate and 0.6 M sodium bicarbonate, to create a buffered pH 7.5 ascorbic acid solution. The dithionite solution consisted of 50 g/L sodium dithionite in 0.35 M acetic acid and 0.2 M sodium citrate, buffered at pH 4.8. All reagents used were ACS grade or better when available. As most samples had low SPM concentration (usually <5 mg/L), the methods were modified for small sample sizes. The PES filters were cut into two equal pieces by ceramic knife and transferred to acid washed 2 ml microcentrifuge vials (FisherScientific®). 1.5 ml of ascorbic solution was added to microcentrifuge vials and samples were placed onto a rotary shaker at 150 rpm in the dark at room temperature for 24 hours. Solutions were centrifuged at 10,000 rpm for 10 minutes and 1 mL of the supernatant was carefully filtered through a 0.22 µm PES syringe filter (Millex®) into a clean 15 mL PP centrifuge tube. Sediments were then rinsed and centrifuged with 1 mL of ultra-pure water (UPW; Milli-Q, 18.2 MΩ cm-1) for 10 minutes, before centrifuging and filtering the supernatant as above. 1.5 mL of the dithionite solution was subsequently added to the sediment and samples were shaken at 150 rpm in the dark at room temperature for 2 hours. The supernatant was filtered through a 0.22 µm PES syringe filter into a clean 15 mL PP centrifuge tube. Three procedural blanks (filters without sediments) were treated as per samples throughout the whole sequential extraction process. Ascorbic and dithionite acid extracts were diluted and acidified in UPW 1:10 to a final concentration of 2% (v/v) HNO_3. Total Fe, Mn and Al were analysed using a Spectro Genesis Inductively Coupled Plasma Optical Emission Spectrometry (ICP-OES) with matrix-matched standards. All concentration (nmol/L)

https://doi.org/10.5194/egusphere-2026-4466
Preprint. Discussion started: 27 August 2026

was divided by water density and data is presented as nmol/kg. Check standards were run along with samples showing good agreement with expected concentrations of Fe and Mn (on average ± 5 %) and higher for Al (on average ± 9 %). Limits of detection (LoD) for ascorbate acid and dithionite extraction solutions were as follows: iron (2 µg/L and 4 µg/L, respectively), Mn (both <0.4 µg/L), and Al concentration (<5 µg/L). Procedural blanks had concentrations close or below the LoD for both extractions. Extract concentrations were above detection limits for both extractions, with median (Q1–Q3) values of FeA 46 (24–166) µg/L and MnA 17 (9–26) µg/L for the ascorbate extraction, and FeD 161 (68–318) µg/L, MnD 2 (1–6) µg/L, and Al 11 (5–21) µg/L for the dithionite extraction.

For selected samples, iron and manganese extractions using the Berger Leach method (Berger et al., 2008) were used to compare with the selective Fe and Mn extractions. A detailed description of the Berger Leach procedure is provided in the Supplementary Methods (Text 1.2), while the corresponding results are presented in Figure S.1.

3.2.2 Analysis of trace elements

Trace elements (Al, Fe, Mn) in seawater were determined using a multi-quadrupole inductively coupled plasma mass spectrometer (PerkinElmer NexION 5000 ICP-MS/MS) (Table S.1). The ICP-MS/MS was operated in KED and DRC modes to remove polyatomic and isobaric interferences in sample matrices. KED mode was operated with He as the collision gas. DRC mode was operated in either on-mass or mass-shift mode with NH_3, O_2 or N_2O as the reaction gases depending on the element of interest (e.g., ^{56}Fe was measured using NH_3 in mass shift mode with Fe forming a Fe-NH_3 cluster at a m/z 90, moving it away from the interfering $^{40}Ca^{16}O$ and $^{40}Ar^{16}O$; (Xing and Stephan, 2022). Field and procedural blanks were below the instrumental limit of detection (LoD) or significantly lower than filtered and unfiltered sample concentrations. Samples were diluted 1:20 prior to analysis due to high salinity, and standards were matrix-matched using ultrapure NaCl (seaBlank, Elemental Scientific Inc.). To assess the quality of the analyses, certified reference materials (NASS-5, CASS-6, and SLEW-4) were used, with elemental recoveries typically within 80-120% of the certified value (Table S.2). The relatively low dFe concentration in NASS-5 (6.16 nmol kg^{-1}), which is only a few times higher than the analytical LoD (1.3 nmol kg^{-1}), likely contributed to the lower recovery and higher analytical uncertainty. LoDs were: Al (2.9 nmol/kg), Fe (1.3 nmol/kg), and Mn (0.2 nmol/kg). The mean and standard deviation of trace element concentrations in field blanks (N=6) were: Al (13.6±9.1 nmol/kg), Fe (1.5±0.3 nmol/kg), Mn (0.6±0.4 nmol/kg). Field blanks were prepared by collecting ultrapure water (UPW) using a pre-cleaned Niskin bottle and transferring it through pre-cleaned silicone tubing following the same procedure as for sample filtration. Procedural blanks were at or below the detection limit. All analyses were performed in a covered autosampler within a class 1000 clean room, and all acids used were in-house, twice distilled, ultrapure grade. Analyses of trace elements were supplemented with macronutrients and organic carbon analyses (see supplementary materials, text S1.3).

3.3 Additional analytical methods

3.3.1 Geochemical analyses

Selected SPM samples were analysed by powder X-ray diffraction (pXRD) and scanning electron microscopy coupled with energy-dispersive X-ray spectroscopy (SEM-EDS) to constrain bulk mineralogy and particle moprhologies and semi quantitative chemical make-up. Dried particulate material was homogenised in an agate mortar and analysed using a STOE Stadi P diffractometer with Cu radiation (lambda = 1.54 A), a DECTRIS

https://doi.org/10.5194/egusphere-2026-4466
Preprint. Discussion started: 27 August 2026

MYTHEN 2 detector and a Ge(111) monochromator. Mineral phases were identified against COD2019 reference patterns using PROFEX, and semi-quantitative assessment was supported by CrystalDiffract 7.0. Note that the collected SPM samples were not rinsed prior to pCRD analyses and thus sea salts (halite) crystalized from seawater, was present in all spectra. SEM-EDS observations were performed on particles collected on 0.22 µm track-etched polycarbonate filters using a Quanta 3D FEG SEM coupled to an EDAX Octane Elect EDS detector. Analyses were conducted at 20 kV, with EDS spectra acquired using a 30 s live time. SEM-EDS results were used as semi-quantitative particle-scale compositional information and interpreted together with pXRD and extraction chemistry. For details see supplementary materials (text S1.4).

3.3.2 Calculation of sedimentation rate including FeA, FeD, MnA, MnD sedimentation

Cumulative sedimentation between 29th June and 22nd August was calculated from nearly continuous measurements of sedimentation rate 5 m above the fjord bottom for both 2022 and 2023 samples. Linear interpolation was used for days with no observations. The sedimentation rate of Fe and Mn was calculated based on the mean (minimum-maximum range) SPM-corrected Fe [% d.w.] and Mn [% d.w.] from the respective summer seasons (2022 and 2023) multiplied by the SPM sedimentation rate. Only samples from the vicinity of sediment traps were used from Hansbukta (HB1 and HB2) and Gåshamna (GH1 and GH2).

3.3.3 Analysis of meteorological data

The air temperature dataset from the Polish Polar Station in Hornsund was downloaded from meteostat.net. The daily average air temperature (AT) was used to calculate the sum of all daily AT values > 0 °C (PDD AT) for six days. The start of the melt season was defined as the start of the first period of 6 consecutive days with AT > 0 °C (modified from Błaszczyk et al., 2021). This takes into account the delays in meltwater and particulate matter delivery to the fjord, and the 6 d window was shown to be well correlated with sediment flux (in this study and D'angelo et al. (2018).

3.3.4 Statistical analyses

Due to the presence of numerous outliers and non-normal distributions of most variables, statistical analyses were predominantly based on non-parametric methods. Relationships between variables were primarily assessed using Spearman's rank correlation coefficient (referred to in the text as ρ), with the p-value < 0.05. In selected cases, where assumptions of parametric analyses were met, Pearson's correlation coefficients (R, p-value < 0.05) and linear regression models were applied. When necessary, relationships were linearized using logarithmic transformations of the variables. For parametric analyses, the normality of model residuals was evaluated using the Kolmogorov–Smirnov test with Lilliefors correction. All statistical analyses were performed using Statistica 13.3 (TIBCO Software Inc.).

3.3.5 Geochemical indices

Highly reactive (FeA, MnA) and more crystalline, less reactive (FeD, MnD) particulate element phases were defined using ascorbic acid and dithionite extractions, following Raiswell et al. (2018); Raiswell et al. (2010) Lenstra et al. (2021); Lenstra et al. (2022). Based on these operationally defined fractions, geochemical indices (FeA:FeD, MnA:MnD) were used to compare the lability of particulate metal pools, while FeA:dFe and MnA:dMn

https://doi.org/10.5194/egusphere-2026-4466
Preprint. Discussion started: 27 August 2026

ratios were applied to assess the relative size of the reactive particulate pool to the filterable fractions (dFe, dMn), commonly considered more bioavailable.

4 Results

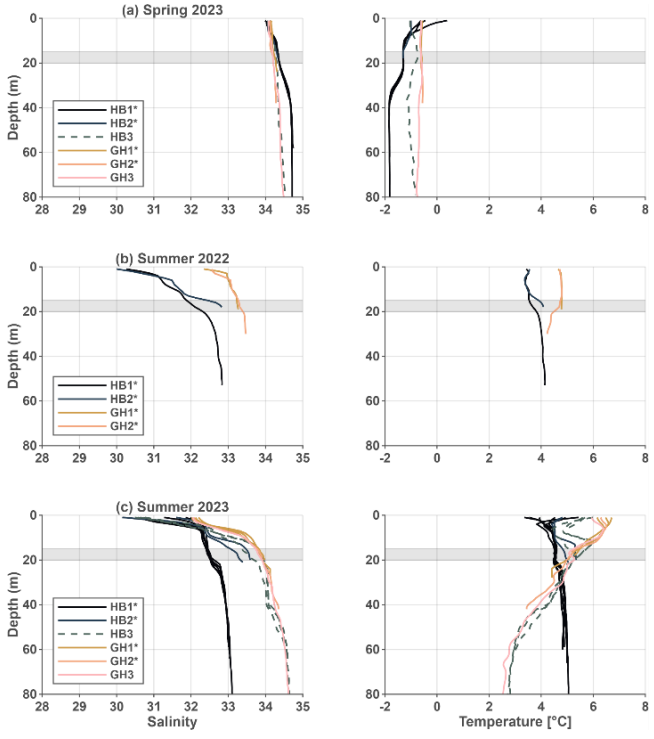

Figure 2. Vertical salinity and temperature profiles in Hansbukta and Gåshamna in May 2023 (a), August 2022 (b), and July-August 2023 (c). The stars after the station names indicate that the locations of the stations slightly varied between cruises or that multiple stations within similar distances from the glacier terminus were sampled (see Fig. 1). The grey shaded area indicates the approximate depth of the bathymetric sill at the mouth of Hansbukta.

4.1. Hydrography and suspended particulate matter

Comparison of the vertical CTD-profiles from the two study locations reveal that the hydrographic properties in Hansbukta and Gåshamna are similar in spring, but clear differences emerge during the melt season (Fig. 2). Close to the terminus of Hansbreen (station HB1), glacier-derived water freshens the entire water column down to the seabed (~90 m, upper 80 m shown in Fig. 2). In 2023, the salinity of the whole water column decreases from around 34.5 in spring to 33 in summer. In Gåshamna, freshening is more modest and limited to the upper 5-10 m, which results in a salinity difference of approximately 1-1.5 between the two basins in both summers 2022 and 2023. However, the shallow sill at the mouth of Hansbukta effectively restricts the freshwater outflow below 20 m, which results in different properties at the outermost station (HB3). HB3 was sampled in summer 2023 when both salinity and temperature resembled those observed in Gåshamna, with a low salinity and temperature signal visible only in the upper 10-20 m layer (Fig. 2C). The bathymetric sill likely restricts the outflow from the glacier, resulting in a large salinity gradient below 20 m between the inner Hansbukta and the station HB3. This vertical

https://doi.org/10.5194/egusphere-2026-4466
Preprint. Discussion started: 27 August 2026

mixing of glacially derived waters in Hansbukta is also observed as weak temperature stratification with temperatures of 4-5 °C throughout the water column (Fig. 3B and C). In contrast, temperatures in Gåshamna, as well as at HB3, range from 3 °C below 60 m to 7 °C at the surface.

Water samples collected during the three cruises reveal that the highest SPM concentrations of 5-10 mg/L are found in the upper 20 m of Hansbukta (Fig. 3). In spring 2023 and summer 2022, the SPM concentrations were lower, at most 5-6 mg/L. Nevertheless, during all three cruises, higher concentrations were observed in Hansbukta compared to Gåshamna (Fig. 3). These differences fit well with seasonal differences of SPM concentration taken throughout the ablation season as a part of the long-term monitoring programme in Hornsund. The water samples collected in the upper 30 m water column during four summers from 2022 to 2025 indicate overall higher SPM concentration in Hansbukta than in Gåshamna despite high interannual and seasonal variability (Fig. 4). The concentration of SPM filtered by GF/F filters (SPM) had a strong correlation with SPM filtered by PES filters (Fig. S.2).

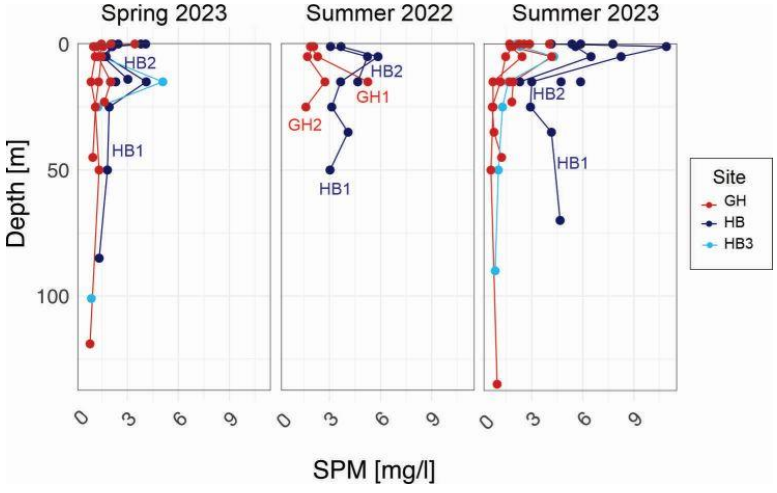

Fig. 3. Suspended particulate matter (in mg/L) concentration in water column profile in Hansbukta (HB) and Gåshamna (GH).

https://doi.org/10.5194/egusphere-2026-4466
Preprint. Discussion started: 27 August 2026

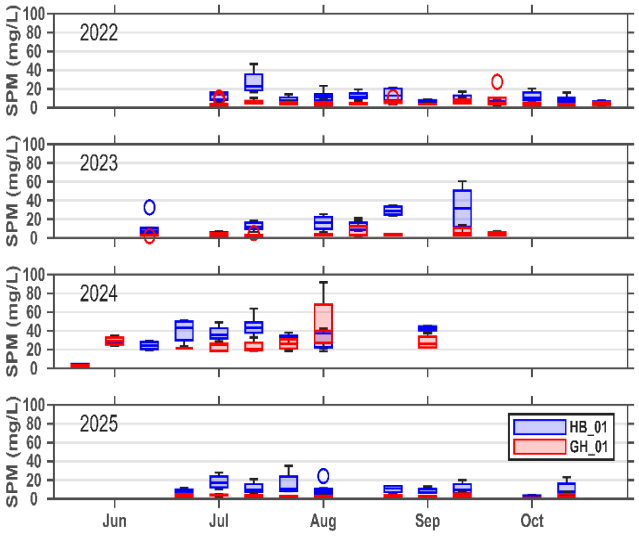

Fig. 4. Suspended Particulate Matter (SPM) concentration in mg/L in Hansbukta (HB) and Gåshamna (GH). The values are averages in the upper 30 m layer over the years 2022-2025, collected as a part of a long term monitoring program. The horizontal line in each box shows the median value, whereas the boxes represent the lower and upper quartiles and the whiskers represent the minimum and maximum values.

https://doi.org/10.5194/egusphere-2026-4466
Preprint. Discussion started: 27 August 2026

4.2. Dissolved and sediment-bound trace elements

4.2.1 Iron

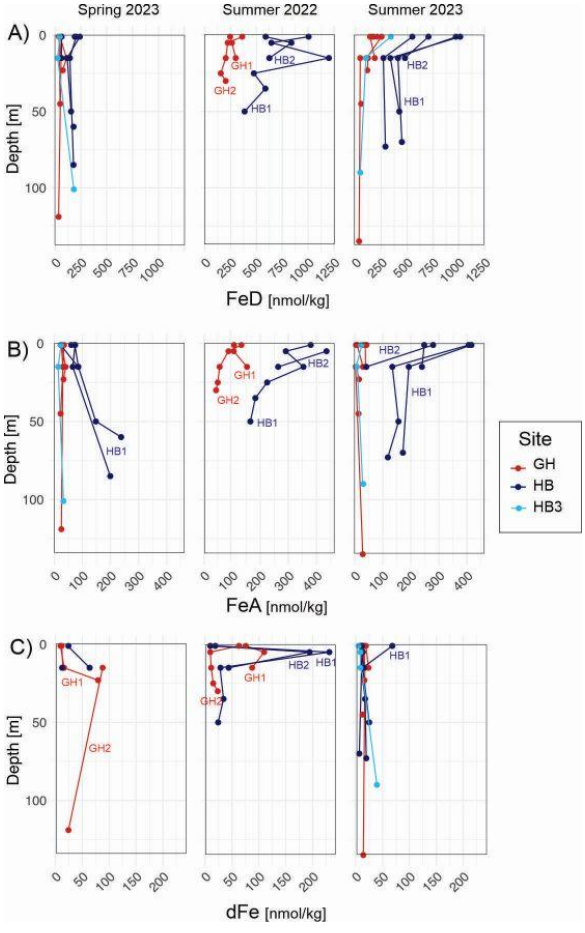

Fig. 5. Sediment-bound and dissolved Fe in nmol/kg in the water column during summer and spring seasons in Hansbukta (HB) and Gåshamna (GH). A) FeD, B) FeA, C) dFe. HB3 is the farthest location in Hansbukta situated behind the sill.

Sediment-bound iron phases (FeD and FeA) were consistently higher than dFe at both sites. Freshwater endmembers exhibited markedly higher FeD (median 5078 nmol/kg for Gåshamna) and FeA (median 594 nmol/kg for Gåshamna) concentrations compared with fjord water (medians for both bays, 46-625 nmol/kg and 22–277 nmol/kg, respectively; Table 1, Fig. 5). In contrast, dFe in freshwater endmembers (0.2–88 nmol/kg), which had alkaline pH (~8.5), fell within the range of fjord concentrations (medians for both bays 12–43 nmol/kg). Comparisons between the two bays highlight systematically higher FeD and FeA in Hansbukta than in Gåshamna, while dFe was slightly lower (Fig. 5). Median FeA and FeD in Hansbukta were approximately three- and sevenfold higher than in Gåshamna. In addition, for SPM-standardized FeA [% d.w.] and FeD [% d.w.] (Figure S.3), a similar pattern was shown. High FeA and FeD patterns align with total dissolvable Fe (TdFe), which exhibited four times

https://doi.org/10.5194/egusphere-2026-4466
Preprint. Discussion started: 27 August 2026

higher Fe concentrations in Hansbukta compared with Gåshamna (Table S.3). Median particulate Fe (FeA and FeD in Hansbukta, and FeD in Gåshamna) concentrations were 2–4-fold higher in summer than spring in both 2022 and 2023 (Table 1).

These contrasts in Fe concentrations motivate the use of geochemical indices to compare dissolved and particulate Fe pools. During summer, FeA:dFe and FeA:FeD were higher in Hansbukta than in Gåshamna (Fig. 6A, B). The reactive particulate Fe (FeA) fraction was substantially higher than the dFe in Hansbukta (median FeA:dFe six-fold higher). The FeA:FeD ratio (~0.4 for Hansbukta in summer) indicates that reactive fractions are about half as abundant as more crystalline fractions. During the spring, there was less spatial variation in concentrations of all Fe phases. Freshwater samples displayed much smaller FeA:FeD ratios (median 0.08), whereas FeA:dFe (~2250) ratios were 2–3 orders of magnitude higher than in seawater (Table S.4).

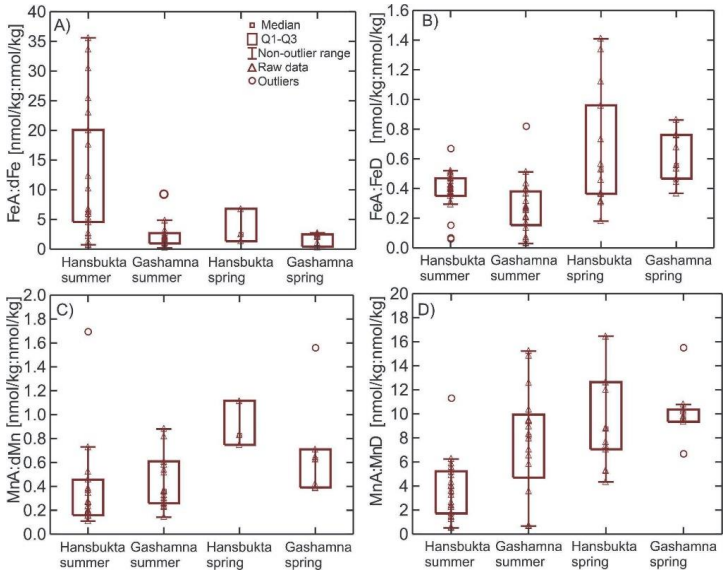

Fig. 6. Comparison between ratios of sediment-bound and dissolved Fe and Mn in Hansbukta and Gåshamna in both summer seasons of 2022 and 2023 and spring season 2023. A) FeA:dFe, B) FeA:FeD, C) MnA:dMn, D) MnA:MnD.

Vertical distributions of Fe further emphasize differences between Hansbukta and Gåshamna. In Hansbukta, surface waters showed the strongest glacier influence, with elevated FeA and FeD (140–450 nmol/kg and 200–1000 nmol/kg, respectively) and decreasing concentrations with depth near Hansbreen (HB1, HB2); (Fig. 5A, B). Although concentrations varied between the summers of 2022 and 2023, with smaller seasonal contrasts in 2023, Hansbukta consistently exhibited higher Fe concentrations throughout the water column than Gåshamna. At more distal sites (HB3, Fig. 5), FeA and FeD decreased throughout the entire profile compared with HB1 and HB2, indicating dilution and/or non-conservative loss along the fjord axis. The dFe concentrations were higher in surface waters, especially in HB in summer, and decreased in concentrations in the lower part of the water column profile (Fig. 5 C).

https://doi.org/10.5194/egusphere-2026-4466
Preprint. Discussion started: 27 August 2026

Table 1. Summary of statistics for dissolved and sediment-bound Fe, Mn and Al in nmol/kg (mean, median (min-max range)).

	Hansbukta			Gåshamna			Seawater	Rivers	
Parameter [nmol/kg]	Summer 2022	Summer 2023	Spring 2023	Summer 2022	Summer 2023	Spring 2023	**all**	Hansbreen*	Gåsbreen
dFe	73.1, **31.5** (9.6-231)	17, **11.7** (5.1-68.1)	33.5, **24.3** (12.6-63.7)	49.5, **43.3** (9.7-109.8)	15.9, **15.9** (12.8-23.7)	34.7, **16.2** (9.5-87.9)	32.2, **16.2** (5.1-231)	88.5	6.3, **0.7** (0.7-17.6)
FeA	287.1, **277.4** (165-435.9)	175.9, **163.8** (6.3-415.7)	86.2, **73.1** (13.6-237.8)	91.6, **96.3** (42.9-153)	21.7, **22.2** (3.4-42.2)	29.6, **30.3** (22.3-40.3)	111.6, **58** (3.4-435.9)	1250.0	691.1, **594.9** (450.7-1027.6)
FeD	705, **624.8** (384.8-1200.9)	456.6, **417.8** (45.7-1013.6)	136.1, **153.8** (24.1-238.1)	243.2, **232.7** (154.2-361.3)	133.5, **131.1** (35-252.7)	53.7, **46.5** (33-109.4)	285.2, **190** (24.1-1200.9)	22106.9	5985.9, **5078.4** (4505-8374.4)
dMn	121.3, **129.8** (99-146.1)	73, **78.4** (10.3-130.6)	15.5, **15.7** (13.8-17)	51.4, **50.7** (30.7-76.7)	55.3, **64** (10.5-97.2)	13.7, **13.9** (11.1-15.2)	63.1, **70.3** (10.3-146.1)	49.9	75.1, **64.5** (3.7-157.1)
MnA	18.5, **18.5** (14.5-24.9)	28, **26.6** (22.6-35.7)	17.1, **13** (7.2-40.5)	15.4, **16** (10.9-18.2)	25.8, **25.7** (16.8-37.9)	8.3, **7.4** (5.5-17.3)	19.8, **18.5** (5.5-40.5)	244.7	91.1, **129.6** (11.8-131.9)
MnD	16.6, **13.1** (5.8-38.2)	6.5, **5.9** (1.5-14.8)	2.0, **1.9** (0.4-3.5)	11.6, **10.4** (2-22.9)	2.5, **2.7** (1.1-3.6)	0.8, **0.9** (0.5-1.4)	5.9, **2.9** (0.4-38.2)	252.0	120.8, **130.5** (75.2-156.7)
dAl	152.3, **130.4** (78.7-310.3)	123.3, **63.6** (38.3-268.2)	125.9, **121.3** (1.4-334.9)	108.4, **57.6** (38.6-459.1)	54.4, **39.2** (1.4-197.5)	97.9, **32.4** (1.4-319.5)	106.8, **70.5** (1.4-459.1)	662.1	652.1, **864.0** (53.5-1038.9)

4.2.2 Manganese

Summer dMn (51-130 nmol/kg) exceeded particulate fractions by factors of ~2 and more for MnA (medians ~16-27 nmol/kg) and ~5 - ~23 for MnD (medians ~3-13 nmol/kg) (Table 1). In contrast, freshwater endmembers had higher sediment-bound Mn (MnA = 130 nmol/kg; MnD = 131 nmol/kg for Gåsbreen) relative to both seawater and freshwater dMn (median 65 nmol/kg MnA for Gåshamna). Hansbukta generally showed higher concentrations of all Mn fractions than Gåshamna, though the contrasts were smaller than for Fe (Fig. 7): dMn and MnD were approximately twice as high in Hansbukta in summer seasons, while MnA was similar. Total dissolvable Mn was ~30% higher in Hansbukta (Table S.3).

Seasonally, both fjord branches exhibited higher Mn in summer than in spring, with the strongest differences for MnD and dMn. In Hansbukta, dMn increased 5-8× between spring and summer, exceeding the more moderate increase in Gåshamna (Table 1, Fig. 7). In summer seawater, Hansbukta exhibited a higher MnA:MnD than Gåshamna (Table S.4), while MnA:dMn ratios (0.25-0.36) were similar across sites (Fig. 6 C, D). During spring, both Mn indices converged and exceeded summer values. Mn indices showed markedly smaller contrasts between freshwater and seawater compared with Fe (Table S.4).

https://doi.org/10.5194/egusphere-2026-4466
Preprint. Discussion started: 27 August 2026

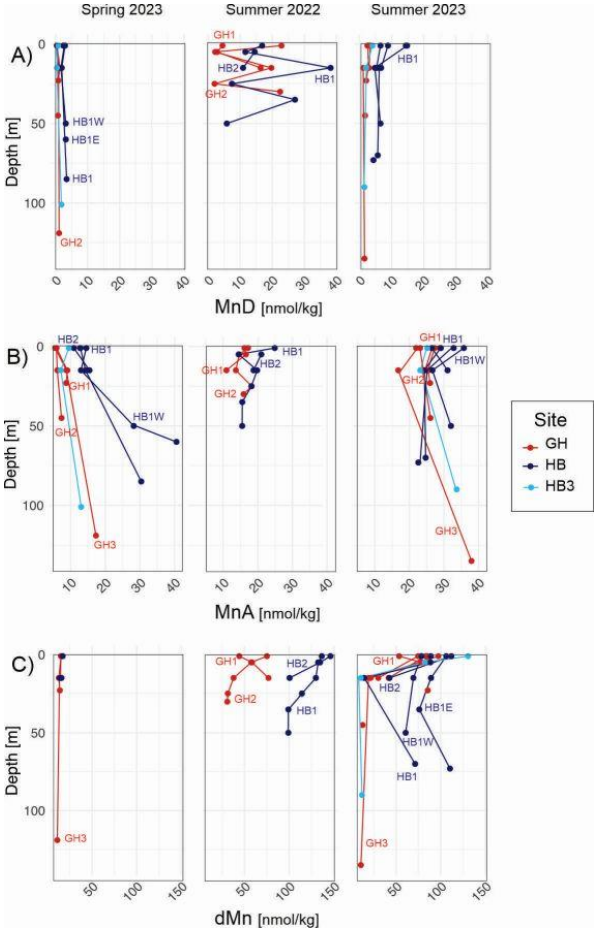

375 **Fig. 7. Sediment-bound and dissolved Mn in nmol/kg in the water column in Hansbukta (HB) and Gåshamna (GH). A) MnD, B) MnA, C) dMn. HB3 is the farthest location in Hansbukta situated behind the sill.**

4.2.3 Differences in iron and manganese behaviour

Particulate Fe fractions in Hansbukta exhibited stronger correlations with SPM, salinity and Mn-related parameters than in Gåshamna, pointing to a more pronounced influence of estuarine mixing and particle supply on particulate
380 iron. At both sites, sediment-bound Fe fractions correlated with SPM (Fig. 8A, 8B), with stronger relationships for FeA in Hansbukta ($\rho = 0.63$, p-value < 0.05, Table S.5), whereas summer showed a stronger correlation (Table S.6). FeD vs. SPM correlations in Hansbukta were comparable to those for FeA, but Gåshamna exhibited much stronger FeD vs. SPM coupling ($\rho = 0.84$, $p < 0.05$; Table S.5), suggesting the delivery of more crystalline particulate material associated with glacial erosion products. FeA and FeD showed consistently strong correlations
385 with MnD ($\rho = 0.7–0.9$, $p < 0.05$) but weaker correlations with MnA (usually $\rho < 0.4$, $p < 0.05$), with the MnD vs. Fe relationships notably stronger and more consistently significant in Hansbukta (Table S.5). This MnD vs. Fe coupling intensifies in Hansbukta during summer ($\rho = 0.86–0.94$, $p < 0.05$ Table S.6). Negative correlations with salinity were stronger for FeD in Hansbukta (FeD $\rho = -0.86$, $p < 0.05$, Table S.5), compared with dFe (Fig. 9C).

https://doi.org/10.5194/egusphere-2026-4466
Preprint. Discussion started: 27 August 2026

Gåshamna displayed a strong summer FeD-dAl correlation ($\rho \approx 0.6$, p-value < 0.05), suggestive of lithogenic inputs (Table S.6). Further details on Al coupling are given in the supplementary materials (Text 2.1; Fig. S.4). Manganese cycling shows coherent, seasonally modulated coupling to lithogenic proxies and mixing. In summer, dAl vs. dMn relationships strengthen when sites are pooled ($\rho = 0.66$, Table S.6, Text S2.1), with only minor site differences and slightly higher ρ at Gåshamna, consistent with enhanced delivery of lithogenic particulates during peak ablation (Table S.6, Fig. S.4). dMn exhibited a clear estuarine-mixing signal in both bays (R with salinity = -0.83 overall, $p < 0.05$, Fig. 9A, Table S.5) with highest concentrations at lower salinity. The dMn intercept (948 nmol/kg) is close to our freshwater endmember value for TdMn (~814 nmol/kg, Table S.3) and higher than the freshwater endmember sum of dMn, MnA, MnD (~653 nmol/kg, when maximum values included, Table 1). This suggests that reactive Mn-bearing particles sourced from glacial erosion are converted to dMn in seawater. In contrast to FeA:FeD (0.3-0.6), MnA:MnD has values above 1 (usually 3.5-10, Table S.4), showing that the highly reactive particulate phase of Mn (MnA) dominates the reactive particulate Mn pool in these environments (Fig. 6C, D).

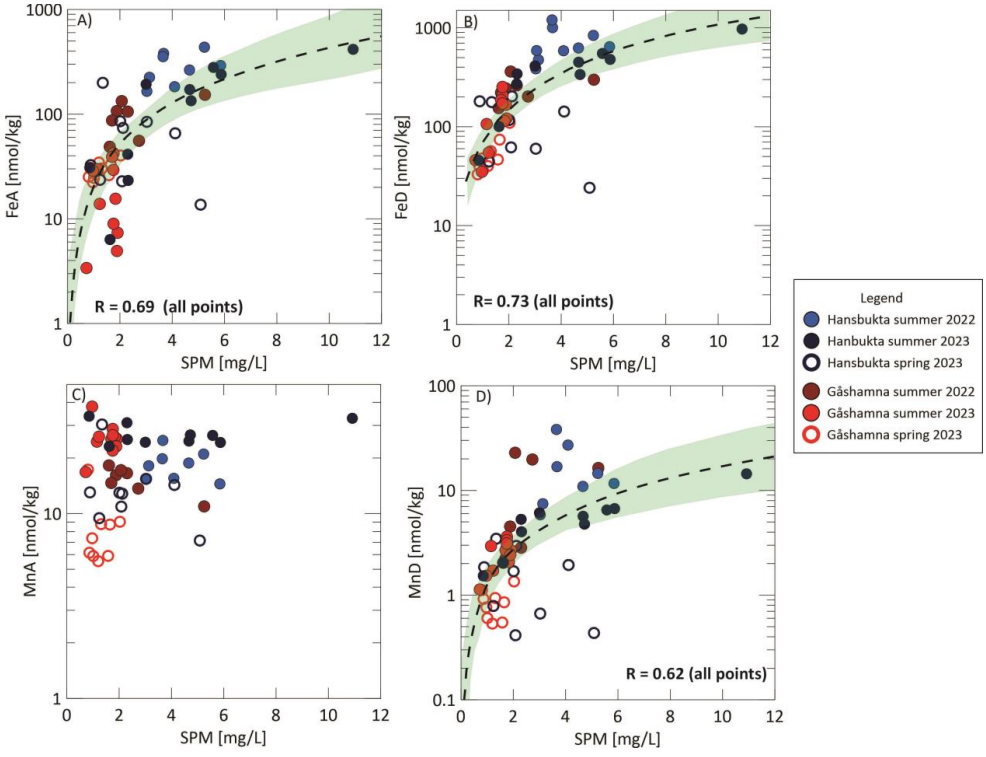

Fig. 8. Relationship between sediment-bound micronutrients and suspended particulate matter (SPM) for Hansbukta and Gåshamna. A) FeA, B) FeD, C) MnA, D) MnD. Shading shows 95% confidence intervals.

https://doi.org/10.5194/egusphere-2026-4466
Preprint. Discussion started: 27 August 2026

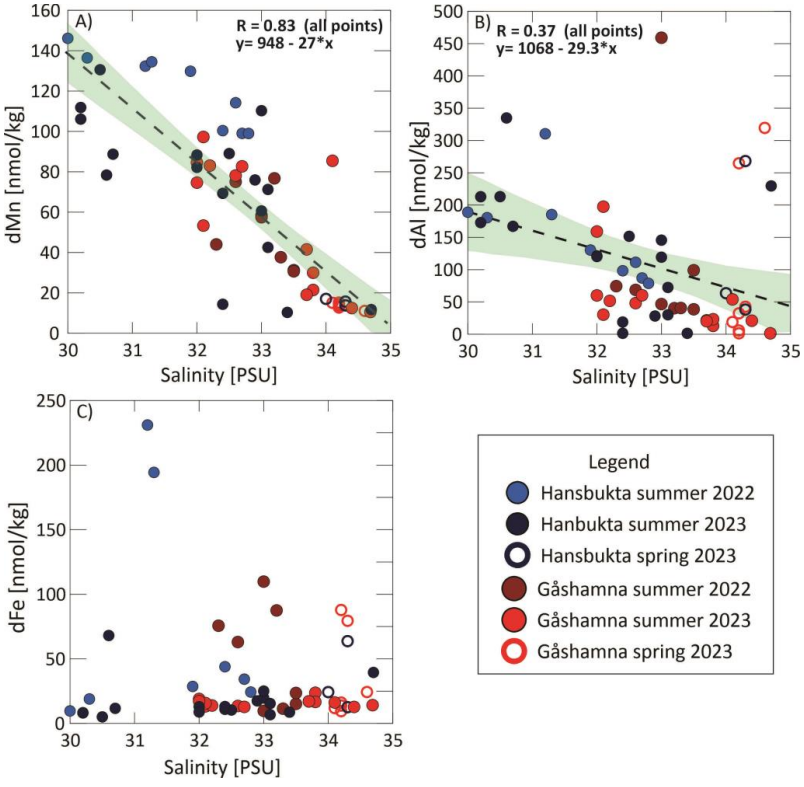

Fig. 9. Relationship between dissolved trace elements and salinity. A) dMn, B) dAl, C) dFe. Shading shows 95% confidence intervals.

4.2.4 Sedimentation of iron and manganese

Consistent with the contrasting particulate Fe and Mn pools described above, ablation-season sedimentation differed sharply between the two fjord basins (Fig. 10). During peak ablation (June–August), cumulative sediment accumulation in Hansbukta 2022 and 2023 (136 kg/m^2 and 99 kg/m^2, respectively) was 33 and 141 times higher than in Gåshamna (4.1 kg/m^2 and 0.7 kg/m^2, respectively), respectively (Fig. 10C). This difference of one to two orders of magnitude reflects the strong intensification of sediment delivery to Hansbukta during summer, while sedimentation in Gåshamna remained persistently low.

Sediment-bound Fe and Mn sedimentation fluxes during the ablation season showed marked differences between Hansbukta and Gåshamna. During the 2022 and 2023 ablation seasons, FeA sedimentation in Hansbukta averaged ~530 g/m^2 and ~220 g/m^2, respectively, exceeding values observed in Gåshamna by more 1-2 orders of magnitude (~10 and ~0.5 g/m^2, respectively Fig. 10A). Sedimentation of the more crystalline Fe fraction (FeD) was typically 2-7 times higher than FeA at both sites, indicating dominance of less reactive particulate phases in the settling SPM. A different tendency was observed for Mn, with MnA sedimentation in Hansbukta averaging ~34–35 g/m^2 in both years, higher than in Gåshamna (~1.6 g/m^2 and ~0.6 g/m^2 in 2022 and 2023, respectively) (Fig. 10B)

https://doi.org/10.5194/egusphere-2026-4466
Preprint. Discussion started: 27 August 2026

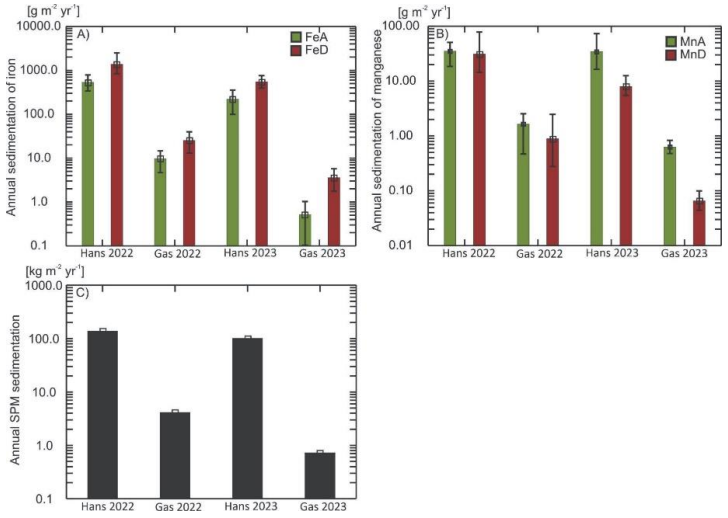

425 **Fig. 10. Sedimentation of FeA and FeD (A), MnA and MnD (B), and SPM (C) in Hansbukta and Gåshamna.**

4.4 XRD analyses and SEM analyses

XRD patterns show that SPM samples from Hansbukta and Gåshamna are dominated by detrital silicate and phyllosilicate minerals. Gåshamna SPM contains, quartz, calcite, dolomite, chlorite and mica, with minor plagioclase, whereas Hansbukta is dominated by quartz, mica and chlorite, dolomite, calcite and plagioclase (Fig.
430 S.5). SEM-EDS observations reveal fine-grained aggregates and coatings with variable Fe enriched phases associated with O-, Al- and Si-bearing particles in Hansbukta. The Fe-rich particles appear as sub-micron sized aggretates most often with non-isometric shapes. The EDS analyses indicate associations with silicates from the glacial SPM (Fig S.6). Although no separate iron phases were identified by pXRD and images or SEM-EDS analyses can only infer morphological and chemical characteristics of phases, these suggest that these Fe-rich
435 aggregates could be poorly ordered Fe-bearing phases.

5. Discussion

5.1 Contrasting micronutrient behavior in bays

5.1.1 Particulate phases dominate Fe export to bays

Highly reactive particulate Fe concentrations in coastal regions are much higher than dissolved fractions as a
440 consequence of finely ground glacial flour delivered from land. Concentrations of highly reactive particulate Fe (FeA, FeD) are 1–2 orders of magnitude lower than concentrations reported in freshwater endmembers (Hawkings et al., 2014; Pryer et al., 2020; Stachnik et al., 2025), but remain about four to ten times higher than dFe in fjord waters (for both sites medians values 58-190 nmol/kg vs 16.2 nmol/kg, Table 1). Transport of FeA and FeD from land, therefore, contributes more substantially to the potentially bioavailable Fe pool in fjord water than dFe.
445 Differences in dissolved macronutrient concentrations, δ^{13}C-POC, and δ^{15}N- PTN between Hansbukta and Gåshamna further infer distinct sources of suspended and dissolved material delivered to each bay (Fig. S.7). High

https://doi.org/10.5194/egusphere-2026-4466
Preprint. Discussion started: 27 August 2026

FeA and FeD in both bays are highly correlated to TdFe in our samples, with TdFe values up to three times higher than other glacierised fjords at similar salinities (Hopwood et al., 2016; Krause et al., 2021).

The river endmember sampled from Gåsbreen appears to have a relatively low concentration of dFe compared to seawater in both bays (6.0 vs 16.2 nmol/kg, Table 1) due to alkaline pH and/or sourcing from snowpack (GH0E, Fig. 1). Lower dFe concentrations in endmember river samples suggest that our freshwater endmember may be underestimated, particularly for the Hasbreen where direct sampling of subglacial water is impossible.

Seawater has concentrations comparable to samples collected close to the glacier terminus in other studies (Hopwood et al., 2016; Kanna et al., 2020; Schroth et al., 2011). However, median values from the outer parts of fjords in Svalbard (2 - 5 nmol/kg, (Shen et al., 2024; Schmidt et al., 2025), Greenland fjords (~4 nmol/kg (Kanna et al., 2020) and Antarctica (~6 nmol/kg, (Krause et al., 2021)) are lower than at our study sites. Potential process responsible for elevated dFe concentrations in fjord waters includes the mobilization of Fe from the particulate to the dissolved pool within sediment plumes, which in some coastal systems exhibits a linear relationship with turbidity (Kanna et al., 2020). The weak relationships between salinity and DOC, PO_4^{3-}, POC, PTN, and $\delta^{13}C$-POC, and $\delta^{15}N$-PTN suggest that non-conservative processes, including biological uptake, particle settling, and particulate-dissolved phase exchange, are occurring in these bays and may also influence micronutrient distributions within the fjord (Fig. S.8).

There was a clear difference in particulate Fe between the marine-terminating glacier (Hansbukta) and land terminating glacier (Gåshamna) bays, demonstrating that the subglacial chemical and physical weathering environment controls reactive Fe inputs and cycling in coastal Arctic environments. In Hansbukta, the ascorbate extractable fraction (FeA) was high in all stations (73-277 nmol/kg) and frequently exceeded dFe concentrations (Fig. 5). The SPM-normalized concentration of FeA was also higher for Hansbukta than Gåshamna (Fig. S.3). FeA is formed during chemical weathering of glacial flour in subglacial drainage systems (Hawkings et al., 2014; Stachnik et al., 2025). Therefore, our data indicates more intense chemical weathering is occurring under the subglacial drainage system of Hansbreen than in Gasbreen. In addition, Berger leach, and TdFe concentrations were also higher in Hanbukta than in Gåshamna, along with elevated concentrations of rock weathering-derived elements (Al, Mn), providing further evidence of more intense chemical weathering under Hansbreen before input to the fjord. The greater contribution of highly reactive particulate Fe to the Fe pool is not confined to the immediate vicinity of the glacier but extended across the bay and persisted beyond the sill (24 nmol/kg at the most distal site), indicating substantial lateral transport despite loss within bays, consistent with observations of a weaker salinity control on particulate Fe than dFe in glacierized fjords (Van Genuchten et al., 2021; Krause et al., 2021; Schroth et al., 2014; Van Der Merwe et al., 2019).

In contrast, Gåshamna exhibits a lower concentration of highly reactive particulate iron. Here, FeA constitutes a small fraction of the reactive iron pool (FeA:FeD ~0.26 in summer) and lower SPM-standarized FeA content (0.13%, Table S.4), indicating that SPM derived from land terminating or partially ice-free catchments is geochemically more mature and depleted in the most reactive Fe phases. This distinction demonstrates that high particulate Fe transport alone does not imply high export potential for highly reactive phases and that larger glaciers, and/or glaciers that terminate in or close to the coastal region represent a disproportionately important source of potentially bioavailable iron. Although previous studies have widely applied dFe and Berger leach extractions as proxies for iron bioavailability in glacierised fjords (Van Der Merwe et al., 2019; Krause et al., 2021; Forsch et al., 2021; Forsch et al., 2025), these approaches do not explicitly resolve the mineralogical and

https://doi.org/10.5194/egusphere-2026-4466
Preprint. Discussion started: 27 August 2026

redox controls that govern the biological accessibility of particulate Fe. The Berger leach method, while useful for identifying reactive Fe pools, integrates multiple Fe phases, is not calibrated to Fe phases, and does not selectively target the most reactive poorly crystalline oxyhydroxides. In contrast, FeA isolates Fe associated with poorly ordered or amorphous Fe phases, which have been shown to contain elevated proportions of Fe(II), are generated through subglacial weathering (Hawkings et al., 2018; Jones et al., 2025) and appear to exhibit high bioavailability (Shoenfelt et al., 2017; Wyatt et al., 2023). Our results demonstrate that FeA responds more sensitively to differences between marine-terminating and land terminating glaciers, bathymetric properties of their bays, proglacial river length, and glacier size. This distinction suggests that reliance on Berger leach or dFe alone may underestimate or obscure the role of particulate Fe export to the fjord.

5.1.2 Manganese delivery from ice to fjord

Our study shows that dMn appears to decrease conservatively at the salinities observed at both study sites. This pattern is consistent with near-conservative dMn-salinity behaviour reported for Greenlandic fjords, where dMn attenuates more slowly than Fe across the mixing zone (Van Genuchten et al., 2022). Similar observations are also made in the Canadian Arctic, with marine-terminating glaciers carrying strong micronutrient signals tied to plume turbidity (and thus to subglacial discharge) (Bhatia et al., 2021). Our marine-terminating site shows higher head-of-fjord dMn than the land-terminating bay; yet negative Mn vs salinity correlations ($R = -0.83$ $p < 0.05$ in Hansbukta and Gåshamna, Fig. 9A) indicate that salinity-driven dilution is the first-order control on the dissolved pool at these salinities, with particle–dissolved exchange superimposed on this conservative trend (Van Genuchten et al., 2022). For a comparable salinity range, our dMn (70.3 nmol/kg, Table 1) values are roughly a factor of two lower than in Kongsfjorden (110-130 nM sedimentary substratum; (Yang et al., 2022), higher than gneissic and basaltic settings in Greenland (<40 nM, (Van Genuchten et al., 2022), more than order of magnitude higher for Antarctic fjords (average 5.5 nmol/kg (Forsch et al., 2021), and more than two orders of magnitude higher than typical open ocean concentrations (0.35 nmol/kg, (Van Hulten et al., 2017). The shape of the mixing curves (concentration-salinity) we observe matches that reported in previous studies (Van Genuchten et al., 2022; Yang et al., 2022).

Particulate Mn concentrations increased down-estuary as salinity rose, indicating scavenging of dMn onto suspended particles; however, unlike Fe, the particulate Mn pool comprised a much smaller share of the total Mn pool (dMn+MnA+MnD). MnA and the MnA:MnD increased at higher salinities (≥33 PSU), and approached the majority of reactive particulate Mn pool. In marine-terminating settings elsewhere, chemically reactive particulate phases (including Mn) are concentrated in surface plumes and decay with distance yet retain comparable fractional lability across particle sizes - evidence for efficient suspension and along-fjord transport (Forsch et al., 2025). Consistent with the Canadian Arctic(Bhatia et al., 2021), the contrast between TdMn and dMn in our surface samples was small - much smaller than for Fe - supporting rapid particle–dissolved exchange of Mn in the estuary. TdMn concentrations fall within a range comparable to those reported for surface waters of the glacierized Canadian Arctic Archipelago (~10-100 nM; (Bhatia et al., 2021). Together, these lines of evidence point to a two-stage Mn pathway: (i) subglacial discharge and mixing raise dMn and particulate Mn at fjord heads with salinity-controlled dilution (Van Genuchten et al., 2022; Bhatia et al., 2021), and (ii) transformation of dMn into MnA phases, or transformation of MnD phases to MnA at high salinities builds a mobile MnA pool that is laterally

https://doi.org/10.5194/egusphere-2026-4466
Preprint. Discussion started: 27 August 2026

advected beyond the inner fjord, offering a plausible, long-range source of potentially bioavailable Mn to outer fjords and the adjacent shelf.

5.1.3 Role of macronutrients and organic matter distributions: implications for micronutrient cycling

Although nutrients and organic matter are not the primary focus of this study, their distributions provide additional context for micronutrient cycling (Fig. S.7, S.8, Text S.2.2). In contrast to dMn, which exhibited a strong salinity dependence, most nutrient and organic matter parameters showed weak or highly variable relationships with salinity. DOC remained relatively constant across the observed salinity range, while DIN and phosphate displayed substantial scatter, indicating that biological uptake and regeneration processes likely overprint conservative mixing. In comparison, DSi exhibited a clearer freshwater signal, particularly in Hansbukta, consistent with DSi input from Hansbreen. The weak salinity dependence of δ^{13}C-POC and δ^{15}N-PTN further suggests that organic matter composition is controlled by multiple sources and transformation processes. Together, these observations indicate that micronutrient cycling in glacierized fjords cannot be interpreted solely through estuarine mixing, but must also consider biological processing, particle transport, and sediment-water interactions.

5.2 Controls on particulate micronutrient delivery at glacier–land and glacier–ocean interfaces

Although glacial catchment size is often assumed to be a first-order control on sediment and micronutrient export (Forsch et al., 2025; Wadham et al., 2010; Hallet et al., 1996), our comparison of the Hansbreen and Gåsbreen systems indicates that catchment size alone cannot explain the observed differences in Fe and Mn biogeochemistry in the fjord. In addition to differences in glacier size and freshwater sources, basin geometry strongly influences hydrography, SPM concentrations, and sediment deposition at each site. The most prominent geomorphological difference between the two study locations is the presence of a shallow bathymetric sill, approximately 15 m deep, at the mouth of Hansbukta, which makes this bay more isolated from the inner fjord than Gåshamna. Consequently, it is not straightforward to infer differences in freshwater discharge from hydrographic observations alone, because water-mass retention and exchange are also strongly affected by the sill.

Nevertheless, the considerably larger glacierized area of Hansbreen compared with Gåsbreen likely results in a substantially larger freshwater flux to Hansbukta. Hansbreen covers 51.3 km^2, whereas Gåsbreen covers only 10.9 km^2, with the total Gåsbreen catchment being 38 km^2. The extensive glacierized area of the Hansbreen system promotes subglacial physical erosion and chemical weathering, and the efficient downstream transport of weathering products, including SPM enriched in reactive Fe and Mn. In contrast, the Gåsbreen catchment is dominated by ice-free terrain, where reduced glaciofluvial activity and partial stabilization by vegetation appear to limit sediment mobilization (Dudek et al., 2023; Ziaja et al., 2016). In addition, sediment produced by land-terminating glaciers may be partly retained in proglacial streams, lakes, or floodplains before reaching coastal waters, reducing the sediment flux from Gåsbreen to Gåshamna (Forsch et al., 2025; Zajączkowski, 2008). Importantly, only marine-terminating glaciers deliver sediment-rich subglacial discharge directly to the ocean through buoyant plumes. This contrast in erosional environment is evident in the SPM concentrations observed in Hansbukta and Gåshamna (Figs. 3 and 4), as well as in the associated differences in nutrient and organic-matter composition (Figs. S.7, S.8). However, observations from summer 2023 show that SPM concentrations were considerably lower at the most distant Hansbukta station, HB3, than at the inner stations (Fig. S.9). This suggests

https://doi.org/10.5194/egusphere-2026-4466
Preprint. Discussion started: 27 August 2026

that the sediment-rich outflow and associated particle aggregation and flocculation processes may be spatially limited and partly constrained by the sill (Fig. 3; supplemnetary text S2.3).

Sedimentation measurements support the proposed contrast between high sediment supply to Hansbukta and more limited sediment delivery to Gåshamna, showing one to two orders of magnitude higher sedimentation rates in Hansbukta than in Gåshamna (Fig. 10). In total, 135 and 99 kg/m^2 of sediment are estimated to have been deposited in Hansbukta in ablation seasons 2022 and 2023, respectively.. Although these measurements cover only about two months, they likely capture much of the main annual depositional season, making the cumulative deposition values comparable in magnitude to the deposition rate of 156 kg/m^2/year reported for Kongsfjorden by Trusel et al. (2010). These high deposition values are consistent with a larger sediment flux from Hansbreen, where sediment-rich subglacial discharge is delivered directly to the bay. We suggest that this supply effect is further enhanced locally by the shallow sill at the mouth of Hansbukta, which likely restricts exchange with the inner fjord, increases the residence time of sediment-rich waters, and promoting deposition of suspended Fe- and Mn-bearing particles. This proposed retention mechanism is consistent with previous studies showing that sills can regulate water-mass exchange and renewal in stratified or glacierized fjords (Farmer and Denton, 1985; Carroll et al., 2017), as well as with recent observations that Hansbukta acts as a "trap" for other trace elements (Pajda et al., 2026).

The contrast between lower SPM concentrations but higher cumulative sediment deposition in 2022 and higher SPM concentrations but lower deposition in 2023 suggests that interannual differences in water-column dynamics also played an important role. Higher SPM concentrations in 2023 indicate that more sediment remained suspended in the water column compared to 2022. However, because salinity was lower in 2022 than in 2023, these differences cannot be directly linked to stronger meltwater discharge from Hansbreen.If the lower salinity observed in 2023 was caused by stronger subglacial discharge, the buoyancy-driven circulation and estuarine exchange within the bay would be expected to intensify (Carroll et al., 2015; Cowton et al., 2015), keeping fine particles in suspension for longer and/or enhancing their export across the sill. Conditions favoring sediment transport over the sill could explain why sedimentation rates were lower in 2023 despite higher SPM concentrations in the water column compared to those observed in 2022. However, the high SPM concentrations observed in 2023 were not associated with lower salinityand therefore the differences in SPM concentrations and sediment deposition between the two years cannot be directly attributed to variations in freshwater discharge. Instead, they may partly reflect differences in the timing of observations relative to melt-season progression. The 2022 survey was conducted in August, when the water column was colder (~4°C) and fresher (<33 PSU), whereas the 2023 survey took place in late July, when waters were warmer (>4°C) and more saline (>33 PSU). Consequently, the lower SPM concentrations but higher sediment deposition in 2022 may indicate that much of the suspended material had already settled by the time of sampling, whereas in 2023 a larger fraction remained in suspension. However, the available hydrographic observations do not allow us to identify the mechanisms responsible for these interannual differences.

FeA and FeD concentrations in suspended particulate matter were 3–7 times higher in Hansbukta than in Gåshamna in the summer seasons (Table 1), highlighting the influence of glacier cover and glacier–ocean connectivity on particulate micronutrient cycling. In contrast, inter-site differences in Mn are less pronounced. Reactive Mn constituted a substantial fraction of the total Mn pool, particularly in high-salinity waters, suggesting efficient redistribution during estuarine mixing. Overall, these results indicate that particulate micronutrient supply

https://doi.org/10.5194/egusphere-2026-4466
Preprint. Discussion started: 27 August 2026

to Arctic fjords is controlled not by catchment area alone, but by the combined influence of glacierized area, glacier terminus type, seabed morphology, sediment composition and concentration, glacier melt and dynamics, proglacial-stream activity, subglacial discharge, and water-mass mixing and retention.

Together, the observed differences between the marine-terminating Hansbreen-Hansbukta system and the land-terminating Gåsbreen-Gåshamna system suggest that micronutrient delivery may follow a non-linear trajectory during glacier retreat, whereby accelerated melting initially enhances erosion, sediment transport, and particulate micronutrient supply, whereas continued glacier shrinkage and transition from marine-terminating to land-terminating conditions may progressively reduce glaciofluvial connectivity, erosive and weathering potential of the ice covered part of the catchment, and direct sediment export to the ocean. Such glacio-hydrological shifts are likely to modify fjord micronutrient reservoirs, affecting benthic biogeochemical processes and the efficiency of micronutrient transfer to the shelf and open ocean (Herbert et al., 2022; Herbert et al., 2020; Laufer-Meiser et al., 2020). Ultimately, the ongoing retreat of Arctic marine-terminating glaciers and the expansion of ice-free catchment areas (Kavan et al., 2025; Kochtitzky et al., 2022) are expected to alter sediment and micronutrient delivery to fjords, with a potential long-term reduction in the terrestrial supply of micronutrients to the ocean.

6 Concluding remarks

This study shows that highly reactive particulate iron represents a major component of the potentially bioavailable Fe pool in glacier-influenced coastal waters, frequently exceeding dissolved Fe concentrations beyond the immediate coastal zone. This underscores the importance of particulate pathways for micronutrient delivery from glacierised catchments to fjords, with flux magnitude governed by glacier size, sediment reactivity, hydrological connectivity, and fjord geometry.

Comparisons between a large and a small glacier system demonstrate that larger glaciers currently exert a disproportionate influence on coastal micronutrient cycling. The larger marine-terminating glacier delivers substantially higher suspended sediment fluxes enriched in labile Fe and Mn and sedimentation rates up to two orders of magnitude greater than those observed in the smaller land-terminating system. These differences suggest more extensive subglacial drainage, stronger physical erosion, prolonged chemical weathering beneath thicker ice, and efficient entrainment of reactive sediments, with fjord bathymetry dictating the retention of sediments and micronutrients. Dissolved Mn concentrations were primarily governed by salinity-driven mixing processes, showing largely conservative behaviour across both systems.

As Arctic glaciers retreat, micronutrient delivery to coastal waters is likely to evolve non-linearly. Early stages of recession and the expansion of active proglacial zones may enhance sediment mobilisation and particulate micronutrient supply, whereas continued glacier shrinkage, increasing ice-free areas, and landscape stabilization will ultimately reduce micronutrient fluxes. Fe is predominantly associated with the reactive particulate phase, while Mn exhibits dynamic coupling between particulate and dissolved pools; the high concentrations of dMn observed in fjord waters indicate that it is largely derived from the particulate pool during low salinity mixing. Consequently, glacier size and the persistence of active subglacial and proglacial processes emerge as key controls on fjord micronutrient reservoirs and their role in shelf and ocean export.

https://doi.org/10.5194/egusphere-2026-4466
Preprint. Discussion started: 27 August 2026

Data availability

The dataset supporting the results presented in this study is publicly available in the Zenodo repository: Stachnik, L., Korhonen, M., Hawkings, J., Koziorowska, K., Kulinski, K., Szymczycha, B., & Moskalik, M. (2026). Biogeochemical properties of seawater and suspended particulate matter in an Arctic fjord under contrasting glacier influence (Hornsund, Svalbard, 2022-2023) [Dataset]. Zenodo. https://doi.org/10.5281/zenodo.21371463

Author contributions

LS conceptualized the study, curated the data, and prepared the original manuscript draft. MK contributed to data curation, investigation, and writing of the original draft. JH contributed to conceptualization, investigation, and writing of the original draft. MS contributed to visualization and methodology. KK contributed to investigation and methodology. ET contributed to visualization and investigation. BS contributed to investigation and funding acquisition. OG contributed to investigation and writing of the original draft. MK contributed to investigation. KDD contributed to investigation. MS contributed to investigation and visualization. LGB contributed to methodology and writing of the original draft. PF contributed to investigation and visualization. MM contributed to conceptualization and funding acquisition. All authors contributed to the interpretation of the results, critically revised the manuscript, and approved the final version of the manuscript.

Competing interests

The authors declare no competing interests.**Acknowledgements**

We would like to thank Laura Bromboszcz-Szczypior and Piotr Prusiński for their support during laboratory measurements and Natalia Gackowska for help in sample collection.

Financial support

The research leading to these results has received funding from the Polish National Science Centre SONATA (FLOURISH, award no. UMO-2021/43/D/ST10/00687), Norwegian Financial Mechanism 2014–2021 projects GRIEG-1 (RAW award no. 2019/34/H/ST10/00504, ArcticSGD award no. 2019/34/H/ST10/00645) and within the statutory activities of the Institute of Oceanology Polish Academy of Science. ŁS was supported by the Bekker Programme (award no. BPN/BEK/2021/1/00431) from the Polish National Agency for Scientific Exchange, and through a project from the National Science Centre in Poland (FLOURISH, award no. UMO-2021/43/D/ST10/00687). This project has received funding from the European Union's Horizon 2020 research and innovation Transnational Access programme EXCITE under grant agreement No 101005611. ŁS acknowledges funding for their transnational Access (TNA id: EXCITE_TNA_C2_2022_008) for research conducted at the Potsdam Imaging and Spectral Analyses (PISA) facility at the Helmholtz-Zentrum Potsdam Deutsches GeoforschungsZentrum, Potsdam Germany. LGB, PF and MS achnowledge support from the Helmholtz Recruiting initiative (award no. I-044-16-01). JH acknowledges funding from the US National Science Foundation (project MEGA award no. 2232980) and the Research Council of Norway through its Centres of Excellence funding scheme, project number 332635 (iC3: Centre for ice, Cryosphere, Carbon and Climate).

https://doi.org/10.5194/egusphere-2026-4466
Preprint. Discussion started: 27 August 2026

References

Achterberg, E. P., Steigenberger, S., Marsay, C. M., LeMoigne, F. A. C., Painter, S. C., Baker, A. R., Connelly, D. P., Moore, C. M., Tagliabue, A., and Tanhua, T.: Iron Biogeochemistry in the High Latitude North Atlantic Ocean, Sci. Rep.-UK, 8, 1283, 10.1038/s41598-018-19472-1, 2018.

Bhatia, M. P., Waterman, S., Burgess, D. O., Williams, P. L., Bundy, R. M., Mellett, T., Roberts, M., and Bertrand, E. M.: Glaciers and Nutrients in the Canadian Arctic Archipelago Marine System, Global Biogeochem. Cy., 35, e2021GB006976, https://doi.org/10.1029/2021GB006976, 2021.

Birkenmajer, K.: Hornsund Spitsbergen 1:75 000 geology, Katowice, Poland1990.

Błaszczyk, M., Jania, J. A., and Kolondra, L.: Fluctuations of tidewater glaciers in Hornsund Fjord (Southern Svalbard) since the beginning of the 20th century, Pol. Polar Res., 34, 327-352, 10.2478/popore-2013-0024, 2013.

Błaszczyk, M., Ignatiuk, D., Uszczyk, A., Cielecka-Nowak, K., Grabiec, M., Jania, J., Moskalik, M., and Walczowski, W.: Freshwater input to the Arctic fjord Hornsund (Svalbard), Polar Res., 38, https://doi.org/10.33265/polar.v38.3506, 2019.

Błaszczyk, M., Jania, J. A., Ciepły, M., Grabiec, M., Ignatiuk, D., Kolondra, L., Kruss, A., Luks, B., Moskalik, M., Pastusiak, T., Strzelewicz, A., Walczowski, W., and Wawrzyniak, T.: Factors Controlling Terminus Position of Hansbreen, a Tidewater Glacier in Svalbard, J. Geophys. Res-Earth, 126, e2020JF005763, https://doi.org/10.1029/2020JF005763, 2021.

Browning, T. and Moore, M.: Global analysis of ocean phytoplankton nutrient limitation reveals high prevalence of co-limitation, Nat. Comm., 14, 10.1038/s41467-023-40774-0, 2023.

Browning, T. J., Achterberg, E. P., Engel, A., and Mawji, E.: Manganese co-limitation of phytoplankton growth and major nutrient drawdown in the Southern Ocean, Nat. Comm., 12, 884, 10.1038/s41467-021-21122-6, 2021.

Cape, M. R., Straneo, F., Beaird, N., Bundy, R. M., and Charette, M. A.: Nutrient release to oceans from buoyancy-driven upwelling at Greenland tidewater glaciers, Nat. Geosci., 12, 34-39, 10.1038/s41561-018-0268-4, 2019.

Carroll, D., Sutherland, D. A., Shroyer, E. L., Nash, J. D., Catania, G. A., and Stearns, L. A.: Modeling Turbulent Subglacial Meltwater Plumes: Implications for Fjord-Scale Buoyancy-Driven Circulation, J. Phys. Oceanogr., 45, 2169-2185, https://doi.org/10.1175/JPO-D-15-0033.1, 2015.

Carroll, D., Sutherland, D. A., Shroyer, E. L., Nash, J. D., Catania, G. A., and Stearns, L. A.: Subglacial discharge-driven renewal of tidewater glacier fjords, J. Geophys. Res-Oceans, 122, 6611-6629, https://doi.org/10.1002/2017JC012962, 2017.

Cowton, T., Slater, D., Sole, A., Goldberg, D., and Nienow, P.: Modeling the impact of glacial runoff on fjord circulation and submarine melt rate using a new subgrid-scale parameterization for glacial plumes, J. Geophys. Res-Oceans, 120, 796-812, https://doi.org/10.1002/2014JC010324, 2015.

Czerny, J., Kieres, A., Manecki, M., and Rajchel, J.: Geological Map of the SW Part of Wedel-Jarlsberg Land, Spitsbergen, Institute of Geology and Mineral Deposits, University of Mining and Metallurgy, Kraków, Poland1992.

Ćwiąkała, J., Moskalik, M., Forwick, M., Wojtysiak, K., Giżejewski, J., and Szczuciński, W.: Submarine geomorphology at the front of the retreating Hansbreen tidewater glacier, Hornsund fjord, southwest Spitsbergen, J. Maps, 14, 123-134, 10.1080/17445647.2018.1441757, 2018.

D'Angelo, A., Giglio, F., Miserocchi, S., Sanchez-Vidal, A., Aliani, S., Tesi, T., Viola, A., Mazzola, M., and Langone, L.: Multi-year particle fluxes in Kongsfjorden, Svalbard, Biogeosciences, 15, 5343-5363, 10.5194/bg-15-5343-2018, 2018.

Dallmann, W. K. and Elvevold, S.: Chapter 7. Bedrock geology, in: Geoscience atlas of Svalbard, edited by: Dallmann, W. K., Norsk Polarinstitutt, 133-174, 2015.

Dudek, J. and Pętlicki, M.: Unlocking archival maps of the Hornsund fjord area for monitoring glaciers of the Sørkapp Land peninsula, Svalbard, Earth Syst. Sci. Data, 15, 3869-3889, 10.5194/essd-15-3869-2023, 2023.

Dudek, J., Wieczorek, I., Suwiński, M. K., and Strzelecki, M. C.: Paraglacial transformation and ice-dammed lake dynamics in a high Arctic glacier foreland, Gåsbreen, Svalbard, Land Degrad. Dev., 34, 4252-4271, 10.1002/ldr.4773, 2023.

https://doi.org/10.5194/egusphere-2026-4466
Preprint. Discussion started: 27 August 2026

Farmer, D. M. and Denton, R. A.: Hydraulic control of flow over the sill in Observatory Inlet, J. Geophys. Res-Oceans, 90, 9051-9068, https://doi.org/10.1029/JC090iC05p09051, 1985.

Forsch, K. O., Ruacho, A., and Aarons, S. M.: Tidewater cycle drives alpine glacial sediment plume geochemistry, Nat. Comm., 16, 10.1038/s41467-025-64731-1, 2025.

Forsch, K. O., Hahn-Woernle, L., Sherrell, R. M., Roccanova, V. J., Bu, K., Burdige, D., Vernet, M., and Barbeau, K. A.: Seasonal dispersal of fjord meltwaters as an important source of iron and manganese to coastal Antarctic phytoplankton, Biogeosciences, 18, 6349-6375, 10.5194/bg-18-6349-2021, 2021.

Halbach, L., Vihtakari, M., Duarte, P., Everett, A., Granskog, M. A., Hop, H., Kauko, H. M., Kristiansen, S., Myhre, P. I., Pavlov, A. K., Pramanik, A., Tatarek, A., Torsvik, T., Wiktor, J. M., Wold, A., Wulff, A., Steen, H., and Assmy, P.: Tidewater Glaciers and Bedrock Characteristics Control the Phytoplankton Growth Environment in a Fjord in the Arctic, Front. Marine Sci., Volume 6 - 2019, 10.3389/fmars.2019.00254, 2019.

Hallet, B., Hunter, L., and Bogen, J.: Rates of erosion and sediment evacuation by glaciers: A review of field data and their implications, Global Planet. Change, 12, 213-235, 1996.

Hawkings, J., Benning, L., Raiswell, R., Kaulich, B., Araki, T., Abyaneh, M., Stockdale, A., Koch-Müller, M., L Wadham, J., and Tranter, M.: Biolabile ferrous iron bearing nanoparticles in glacial sediments, Earth Planet. Sc. Lett., 493, 92-101, https://doi.org/10.1016/j.epsl.2018.04.022, 2018.

Hawkings, J. R., Wadham, J. L., Tranter, M., Raiswell, R., Benning, L. G., Statham, P. J., Tedstone, A., Nienow, P., Lee, K., and Telling, J.: Ice sheets as a significant source of highly reactive nanoparticulate iron to the oceans, Nat. Commun., 5, 1-8, https://doi.org/10.1038/ncomms4929, 2014.

Hawkings, J. R., Bradley, J. A., Doting, E. L., Hassan, N., Hendry, K. R., Holt, A. D., Hood, E., Spencer, R. G. M., Stibal, M., Tranter, M., Venturelli, R. A., Wadham, J. L., and Bhatia, M. P.: Glacier biogeochemical cycling and downstream impacts, Nat. Rev. Earth Environ., 7, 124-143, 10.1038/s43017-025-00751-1, 2026.

Hawley, R., Mahaffey, C., Hopkins, J., Norman, L., Flanagan, O., Rynders, S., Barton, B. I., Sanders, R. N. C., Meredith, M. P., Arrowsmith, C., and Lohan, M. C.: Iron and Manganese Cycling in the Atlantifying Barents Sea: Concentrated Inputs and Emerging Limitations, Global Biogeochem. Cy., 40, e2025GB009031, https://doi.org/10.1029/2025GB009031, 2026.

Herbert, L. C., Michaud, A. B., Laufer-Meiser, K., Hoppe, C. J. M., Zhu, Q., Aller, R. C., Jørgensen, B. B., and Wehrmann, L. M.: Tight benthic-pelagic coupling drives seasonal and interannual changes in iron-sulfur cycling in Arctic fjord sediments (Kongsfjorden, Svalbard), J. Marine Syst., 225, 10.1016/j.jmarsys.2021.103645, 2022.

Herbert, L. C., Riedinger, N., Michaud, A. B., Laufer, K., Røy, H., Jørgensen, B. B., Heilbrun, C., Aller, R. C., Cochran, J. K., and Wehrmann, L. M.: Glacial controls on redox-sensitive trace element cycling in Arctic fjord sediments (Spitsbergen, Svalbard), Geochim. Cosmochim. Ac., 271, 33-60, https://doi.org/10.1016/j.gca.2019.12.005, 2020.

Hopwood, M. J., Carroll, D., Browning, T. J., Meire, L., Mortensen, J., Krisch, S., and Achterberg, E. P.: Non-linear response of summertime marine productivity to increased meltwater discharge around Greenland, Nat. Commun., 9, 3256, 10.1038/s41467-018-05488-8, 2018.

Hopwood, M. J., Connelly, D. P., Arendt, K. E., Juul-Pedersen, T., Stinchcombe, M. C., Meire, L., Esposito, M., and Krishna, R.: Seasonal changes in Fe along a glaciated Greenlandic fjord, Front. Earth Sci., 4, 1-13, 10.3389/feart.2016.00015, 2016.

Hopwood, M. J., Carroll, D., Dunse, T., Hodson, A., Holding, J. M., Iriarte, J. L., Ribeiro, S., Achterberg, E. P., Cantoni, C., Carlson, D. F., Chierici, M., Clarke, J. S., Cozzi, S., Fransson, A., Juul-Pedersen, T., Winding, M. H. S., and Meire, L.: Review article: How does glacier discharge affect marine biogeochemistry and primary production in the Arctic?, Cryosphere, 14, 1347-1383, 10.5194/tc-14-1347-2020, 2020.

Hugonnet, R., McNabb, R., Berthier, E., Menounos, B., Nuth, C., Girod, L., Farinotti, D., Huss, M., Dussaillant, I., Brun, F., and Kääb, A.: Accelerated global glacier mass loss in the early twenty-first century, Nature, 592, 726-731, 10.1038/s41586-021-03436-z, 2021.

Jones, R. L., Hawkings, J. R., Meredith, M. P., Lohan, M. C., Moore, O. W., Sherrell, R. M., Fitzsimmons, J. N., Kazemian, M., Araki, T., Kaulich, B., and Annett, A. L.: Antarctic glaciers

https://doi.org/10.5194/egusphere-2026-4466
Preprint. Discussion started: 27 August 2026

export carbon-stabilised iron(II)-rich particles to the surface Southern Ocean, Nat. Comm., 16, 10.1038/s41467-025-59981-y, 2025.

Kanna, N., Sugiyama, S., Fukamachi, Y., Nomura, D., and Nishioka, J.: Iron Supply by Subglacial Discharge Into a Fjord Near the Front of a Marine-Terminating Glacier in Northwestern Greenland, Global Biogeochem. Cy., 34, 10.1029/2020GB006567, 2020.

Kavan, J., Szczypińska, M., Kochtitzky, W., Farquharson, L., Bendixen, M., and Strzelecki, M. C.: New coasts emerging from the retreat of Northern Hemisphere marine-terminating glaciers in the twenty-first century, Nat. Clim. Change, 15, 528-537, 10.1038/s41558-025-02282-5, 2025.

Kochtitzky, W., Copland, L., Van Wychen, W., Hugonnet, R., Hock, R., Dowdeswell, J. A., Benham, T., Strozzi, T., Glazovsky, A., Lavrentiev, I., Rounce, D. R., Millan, R., Cook, A., Dalton, A., Jiskoot, H., Cooley, J., Jania, J., and Navarro, F.: The unquantified mass loss of Northern Hemisphere marine-terminating glaciers from 2000–2020, Nat. Comm., 13, 5835, 10.1038/s41467-022-33231-x, 2022.

Korhonen, M., Moskalik, M., Głowacki, O., and Jain, V.: Oceanographic monitoring in Hornsund fjord, Svalbard, Earth Syst. Sci. Data, 16, 4511-4527, 10.5194/essd-16-4511-2024, 2024.

Krause, J., Hopwood, M. J., Höfer, J., Krisch, S., Achterberg, E. P., Alarcón, E., Carroll, D., González, H. E., Juul-Pedersen, T., Liu, T., Lodeiro, P., Meire, L., and Rosing, M. T.: Trace Element (Fe, Co, Ni and Cu) Dynamics Across the Salinity Gradient in Arctic and Antarctic Glacier Fjords, Front. Earth Sci., 9, 10.3389/feart.2021.725279, 2021.

Krisch, S., Browning, T. J., Graeve, M., Ludwichowski, K.-U., Lodeiro, P., Hopwood, M. J., Roig, S., Yong, J.-C., Kanzow, T., and Achterberg, E. P.: The influence of Arctic Fe and Atlantic fixed N on summertime primary production in Fram Strait, North Greenland Sea, Sci. Rep.-UK, 10, 15230, 10.1038/s41598-020-72100-9, 2020.

Laufer-Meiser, K., Michaud, A., Maisch, M., Byrne, J., Kappler, A., Patterson, M., Røy, H., and Jørgensen, B.: Bioavailable iron produced through benthic cycling in glaciated Arctic fjords (Svalbard), Nat. Commun., 12, https://doi.org/10.2343/geochemj.1.014110.1038/s41467-021-21558-w, 2020.

Lenstra, W. K., Klomp, R., Molema, F., Behrends, T., and Slomp, C. P.: A sequential extraction procedure for particulate manganese and its application to coastal marine sediments, Chem. Geol., 584, 120538, 10.1016/j.chemgeo.2021.120538, 2021.

Lenstra, W. K., van Helmond, N. A. G. M., Żygadłowska, O. M., van Zummeren, R., Witbaard, R., and Slomp, C. P.: Sediments as a Source of Iron, Manganese, Cobalt and Nickel to Continental Shelf Waters (Louisiana, Gulf of Mexico), Front. Marine Sci., 9, 10.3389/fmars.2022.811953, 2022.

Lenstra, W. K., Séguret, M. J. M., Behrends, T., Groeneveld, R. K., Hermans, M., Witbaard, R., and Slomp, C. P.: Controls on the shuttling of manganese over the northwestern Black Sea shelf and its fate in the euxinic deep basin, Geochim. Cosmochim. Ac., 273, 177-204, https://doi.org/10.1016/j.gca.2020.01.031, 2020.

Meire, L., Mortensen, J., Meire, P., Juul-Pedersen, T., Sejr, M. K., Rysgaard, S., Nygaard, R., Huybrechts, P., and Meysman, F. J. R.: Marine-terminating glaciers sustain high productivity in Greenland fjords, Glob. Change Biol., 23, 5344-5357, 10.1111/gcb.13801, 2017.

Meire, L., Meire, P., Struyf, E., Krawczyk, D. W., Arendt, K. E., Yde, J. C., Juul Pedersen, T., Hopwood, M. J., Rysgaard, S., and Meysman, F. J. R.: High export of dissolved silica from the Greenland Ice Sheet, Geophys. Res. Lett., 43, 9173-9182, https://doi.org/10.1002/2016GL070191, 2016.

Moskalik, M., Ćwiąkała, J., Szczuciński, W., Dominiczak, A., Głowacki, O., Wojtysiak, K., and Zagórski, P.: Spatiotemporal changes in the concentration and composition of suspended particulate matter in front of Hansbreen, a tidewater glacier in Svalbard, Oceanologia, 60, 446-463, https://doi.org/10.1016/j.oceano.2018.03.001, 2018.

Ng, H. C., Hawkings, J., Bertrand, S., Summers, B., Sieber, M., Conway, T., Sales de Freitas, F., Ward, J., Pryer, H., Wadham, J., Arndt, S., and Hendry, K.: Benthic Dissolved Silicon and Iron Cycling at Glaciated Patagonian Fjord Heads, Global Biogeochem. Cy., 36, 10.1029/2022GB007493, 2022.

Nuth, C., Hagen, J., Kohler, J., Kääb, A., König, M., Moholdt, G., Pettersson, R., and von Deschwanden A.: GLIMS Glacier Database, http://dx.doi.org/10.7265/N5V98602, 2015.

https://doi.org/10.5194/egusphere-2026-4466
Preprint. Discussion started: 27 August 2026

Pajda, B., Moskalik, M., and Zaborska, A.: Glacial bay as a local hot spot for retention and accumulation of heavy metals transported with glacier meltwater (Hornsund, Svalbard), Oceanologia, 68, 10.5697/WCPQ5217, 2026.

Patel, L. K., Głowacki, O., Jain, V., and Moskalik, M.: Assessing Glacier Dynamics and Debris-Cover-Controlled Ablation in Svalbard: Insights from Gåsbreen (2003−2023), Cold Reg. Sci. Technol., 249, 104992, https://doi.org/10.1016/j.coldregions.2026.104992, 2026.

Piret, L., Hawkings, J. R., Hopf, L., and McCabe, D.: Environmental Controls on the Cycling of Fe and Mn in Patagonian Fjord Systems, J. Geophys. Res-Biogeo., 131, 10.1029/2025JG009378, 2026.

Pryer, H. V., Hawkings, J., L., W. J., Robinson, L. F., Hendry, K., Hatton, J. E., Kellerman, A. M., Bertrand, S., Gill-Olivas, B., Marshall, M. C., R.A., B., Daneri, G., and Häussermann, V.: The Influence of Glacial Cover on Riverine Silicon and Iron Exports in Chilean Patagonia, Global Biogeochem. Cy., 34, e2020GB006611, https://doi.org/10.1029/2020gb006611, 2020.

Raiswell, R., Vu, H. P., Brinza, L., and Benning, L. G.: The determination of labile Fe in ferrihydrite by ascorbic acid extraction: Methodology, dissolution kinetics and loss of solubility with age and de-watering, Chem. Geol., 278, 70-79, https://doi.org/10.1016/j.chemgeo.2010.09.002, 2010.

Raiswell, R., Hawkings, J., Elsenousy, A., Death, R., Tranter, M., and Wadham, J.: Iron in Glacial Systems: Speciation, Reactivity, Freezing Behavior, and Alteration During Transport, Front. Earth Sci., 6, 10.3389/feart.2018.00222, 2018.

Ryan-Keogh, T. J., Macey, A. I., Nielsdóttir, M. C., Lucas, M. I., Steigenberger, S. S., Stinchcombe, M. C., Achterberg, E. P., Bibby, T. S., and Moore, C. M.: Spatial and temporal development of phytoplankton iron stress in relation to bloom dynamics in the high-latitude North Atlantic Ocean, Limnol. Oceanogr., 58, 533-545, https://doi.org/10.4319/lo.2013.58.2.0533, 2013.

Schmidt, C. E., Pröfrock, D., Steinhoefel, G., Stichel, T., Mears, C., Wehrmann, L. M., and Thomas, H.: The Contrasting Role of Marine- and Land-Terminating Glaciers on Biogeochemical Cycles in Kongsfjorden, Svalbard, Global Biogeochem. Cy., 39, e2023GB008087, https://doi.org/10.1029/2023GB008087, 2025.

Schmidt, L. S. and Schuler, T. V.: Runoff simulations for Svalbard, 1991-2023 [dataset], https://doi.org/10.21334/NPOLAR.2024.87FA4A0A, 2024.

Schmidt, L. S., Schuler, T. V., Thomas, E. E., and Westermann, S.: Meltwater runoff and glacier mass balance in the high Arctic: 1991–2022 simulations for Svalbard, Cryosphere, 17, 2941-2963, https://doi.org/10.5194/tc-17-2941-2023, 2023.

Schroth, A. W., Crusius, J., Hoyer, I., and Campbell, R.: Estuarine removal of glacial iron and implications for iron fluxes to the ocean, Geophys. Res. Lett., 41, 3951-3958, 10.1002/2014gl060199, 2014.

Schroth, A. W., Crusius, J., Chever, F., Bostick, B. C., and Rouxel, O. J.: Glacial influence on the geochemistry of riverine iron fluxes to the Gulf of Alaska and effects of deglaciation, Geophys. Res. Lett., 38, L16605, 10.1029/2011gl048367, 2011.

Shen, Z., Zhang, R., Ren, J., Marsay, C., Zhu, Z., Wu, Y., Zhang, J., and John, S.: Distribution of dissolved aluminum and dissolved iron in Kongsfjorden: A glacial fjord in the Arctic, Mar. Chem., 263-264, 104399, https://doi.org/10.1016/j.marchem.2024.104399, 2024.

Shoenfelt, E. M., Sun, J., Winckler, G., Kaplan, M. R., Borunda, A. L., Farrell, K. R., Moreno, P. I., Gaiero, D. M., Recasens, C., Sambrotto, R. N., and Bostick, B. C.: High particulate iron(II) content in glacially sourced dusts enhances productivity of a model diatom, Sci. Adv., 3, e1700314, https://doi.org/10.1126/sciadv.1700314, 2017.

Stachnik, L., Hawkings, J., Spolaor, A., Stachniak, K., Ignatiuk, D., Sitek, S., Janik, K., Łepkowska, E., Burgay, F., Syczewski, M. D., Segato, D., Forjanes, P., and Benning, L. G.: Controls of sediment-bound and dissolved nutrient transport from a glacierised metasedimentary catchment in the high Arctic, Chem. Geol., 691, 122940, https://doi.org/10.1016/j.chemgeo.2025.122940, 2025.

Statham, P. J., Skidmore, M., and Tranter, M.: Inputs of glacially derived dissolved and colloidal iron to the coastal ocean and implications for primary productivity, Global Biogeochem. Cy., 22, 10.1029/2007GB003106, 2008.

Tagliabue, A., Bowie, A. R., Boyd, P. W., Buck, K. N., Johnson, K. S., and Saito, M. A.: The integral role of iron in ocean biogeochemistry, Nature, 543, 51-59, 10.1038/nature21058, 2017.

Trusel, L. D., Powell, R. D., Cumpston, R. M., and Brigham-Grette, J.: Modern glacimarine processes and potential future behaviour of Kronebreen and Kongsvegen polythermal tidewater glaciers,

https://doi.org/10.5194/egusphere-2026-4466
Preprint. Discussion started: 27 August 2026

Kongsfjorden, Svalbard, Geological Society, London, Special Publications, 344, 89-102, doi:10.1144/SP344.9, 2010.

van der Merwe, P., Wuttig, K., Holmes, T., Trull, T. W., Chase, Z., Townsend, A. T., Goemann, K., and Bowie, A. R.: High Lability Fe Particles Sourced From Glacial Erosion Can Meet Previously Unaccounted Biological Demand: Heard Island, Southern Ocean, Front. Marine Sci., Volume 6 - 2019, 10.3389/fmars.2019.00332, 2019.

van Genuchten, C. M., Rosing, M. T., Hopwood, M. J., Liu, T., Krause, J., and Meire, L.: Decoupling of particles and dissolved iron downstream of Greenlandic glacier outflows, Earth Planet. Sc. Lett., 576, 117234, https://doi.org/10.1016/j.epsl.2021.117234, 2021.

van Genuchten, C. M., Hopwood, M. J., Liu, T., Krause, J., Achterberg, E. P., Rosing, M. T., and Meire, L.: Solid-phase Mn speciation in suspended particles along meltwater-influenced fjords of West Greenland, Geochim. Cosmochim. Ac., 326, 180-198, https://doi.org/10.1016/j.gca.2022.04.003, 2022.

van Hulten, M., Middag, R., Dutay, J. C., de Baar, H., Roy-Barman, M., Gehlen, M., Tagliabue, A., and Sterl, A.: Manganese in the west Atlantic Ocean in the context of the first global ocean circulation model of manganese, Biogeosciences, 14, 1123-1152, 10.5194/bg-14-1123-2017, 2017.

Wadham, J. L., Tranter, M., Skidmore, M., Hodson, A. J., Priscu, J., Lyons, W. B., Sharp, M., Wynn, P., and Jackson, M.: Biogeochemical weathering under ice: Size matters, Global Biogeochem. Cy., 24, GB3025, https://doi.org/10.1029/2009gb003688, 2010.

Wehrmann, L. M., Formolo, M. J., Owens, J. D., Raiswell, R., Ferdelman, T. G., Riedinger, N., and Lyons, T. W.: Iron and manganese speciation and cycling in glacially influenced high-latitude fjord sediments (West Spitsbergen, Svalbard): Evidence for a benthic recycling-transport mechanism, Geochim. Cosmochim. Ac., 141, 628-655, https://doi.org/10.1016/j.gca.2014.06.007, 2014.

Wyatt, N. J., Birchill, A., Ussher, S., Milne, A., Bouman, H. A., Shoenfelt Troein, E., Pabortsava, K., Wright, A., Flanagan, O., Bibby, T. S., Martin, A., and Moore, C. M.: Phytoplankton responses to dust addition in the Fe–Mn co-limited eastern Pacific sub-Antarctic differ by source region, P Natl. Acad. Sci. USA, 120, e2220111120, 10.1073/pnas.2220111120, 2023.

Xing, L. and Stephan, C.: Direct Analysis of Trace Elements in Open-Ocean Seawater Using the NexION 5000 ICP-MS, 10.13140/RG.2.2.14085.46567, 2022.

Yang, Y., Ren, J., and Zhu, Z.: Distributions and Influencing Factors of Dissolved Manganese in Kongsfjorden and Ny-Ålesund, Svalbard, ACS Earth Space Chem., 6, 1259-1268, 10.1021/acsearthspacechem.1c00388, 2022.

Zajączkowski, M.: Sediment supply and fluxes in glacial and outwahs fjords, Kongsfjorden and Adventfjorden, Svalbard, Pol. Polar Res., 29, 59-72, 2008.

Ziaja, W., Dudek, J., and Ostafin, K.: Landscape transformation under the Gåsbreen glacier recession since 1899, southwestern Spitsbergen, Pol. Polar Res., 37, 155-172, 10.1515/popore-2016-0010, 2016.